

Transcription factor achaete-scute homologue 2 initiates follicular T-helper-cell development

Xindong Liu^{1,2}, Xin Chen¹, Bo Zhong²†, Aibo Wang^{1,2}, Xiaohu Wang^{1,2}, Fuliang Chu³, Roza I. Nurieva², Xiaowei Yan⁴, Ping Chen⁵, Laurens G. van der Flier⁶†, Hiroko Nakatsukasa⁷, Sattva S. Neelapu³, Wanjun Chen⁷, Hans Clevers⁶, Qiang Tian⁴, Hai Qi¹, Lai Wei⁸ & Chen Dong^{1,2}

In immune responses, activated T cells migrate to B-cell follicles and develop into follicular T-helper (T_{FH}) cells, a recently identified subset of CD4⁺ T cells specialized in providing help to B lymphocytes in the induction of germinal centres^{1,2}. Although Bcl6 has been shown to be essential in T_{FH}-cell function, it may not regulate the initial migration of T cells³ or the induction of the T_{FH} program, as exemplified by C-X-C chemokine receptor type 5 (CXCR5) upregulation⁴. Here we show that expression of achaete-scute homologue 2 (Ascl2)—a basic helix-loop-helix (bHLH) transcription factor⁵—is selectively upregulated in T_{FH} cells. Ectopic expression of Ascl2 upregulates CXCR5 but not Bcl6, and downregulates C-C chemokine receptor 7 (CCR7) expression in T cells *in vitro*, as well as accelerating T-cell migration to the follicles and T_{FH}-cell development *in vivo* in mice. Genome-wide analysis indicates that Ascl2 directly regulates T_{FH}-related genes whereas it inhibits expression of T-helper cell 1 (T_{H1}) and T_{H17} signature genes. Acute deletion of Ascl2, as well as blockade of its function with the Id3 protein in CD4⁺ T cells, results in impaired T_{FH}-cell development and germinal centre response. Conversely, mutation of Id3, known to cause antibody-mediated autoimmunity, greatly enhances T_{FH}-cell generation. Thus, Ascl2 directly initiates T_{FH}-cell development.

The development of T_{FH} cells is initiated by and dependent on their movement out of the T-cell zone and into the B-cell follicle. This migration process is regulated by upregulation of CXCR5 as well as downregulation of both CCR7 and P-selectin glycoprotein ligand 1 (PSGL1)^{2,6}. T_{FH} cells have unique developmental regulation and Bcl6 was reported to be selectively expressed in T_{FH} cells^{7–9}. However, although Bcl6 potentiates T_{FH}-cell generation *in vivo*, recent data suggest that it may not regulate CXCR5 upregulation by activated T cells or their migration to B-cell follicles *in vivo*^{3,4}. Hence, the transcriptional mechanisms underlying initial T_{FH}-cell commitment remain unclear⁴.

Recently, we observed that a bHLH-domain-containing transcription factor, Ascl2, was highly expressed in CXCR5^{hi}Bcl6^{hi} cells in comparison with CXCR5[−]Bcl6[−] T cells⁴. Interestingly, CXCR5⁺Bcl6^{lo} T cells also exhibited upregulation of Ascl2 messenger RNA expression⁴, suggesting that its upregulation may precede that of Bcl6. Moreover, the Ascl2 gene locus was marked with active chromatin marker trimethylated histone H3 lysine 4 (H3K4me3) in T_{FH} and, to a much less extent, T_{H2} cells, but not in other T-cell subsets, whereas the other T_{FH}-regulating genes Bcl6 (refs 7–9), Maf¹⁰, Batf^{11,12} and Irf4 (ref. 13) were uniformly associated with H3K4me3 in all T-cell subsets (Extended Data Fig. 1a). To validate these results, we sorted three subpopulations of cells (CXCR5[−]RFP[−], CXCR5⁺RFP^{lo} and CXCR5^{hi}RFP^{hi}; RFP, red fluorescent protein) from Bcl6-RFP reporter mice immunized with keyhole limpet haemocyanin (KLH) emulsified with complete Freund's adjuvant (CFA) (Fig. 1a), and found that Ascl2 was highly expressed

in T_{FH} cells at both mRNA and protein levels (Fig. 1b and Extended Data Fig. 1b). Also, Ascl2 expression was closely correlated with that of CXCR5 (Fig. 1b) and was higher in T_{FH} cells than in other T-cell subsets (Fig. 1c). In human T cells, expression of Ascl2 as well as CXCR5 and Bcl6 was found in human tonsil CXCR5^{hi}PDI^{hi}T_{FH} cells (Fig. 1d, e). Collectively, these results suggest that Ascl2 is highly expressed in T_{FH} cells and that its expression may precede that of Bcl6.

Bcl6 and Batf are necessary in T_{FH}-cell development^{6,12}, whereas Stat5 inhibits T_{FH}-cell development^{14,15}. Overexpression of Bcl6 or Batf, or Stat5 deficiency, failed to increase Ascl2 expression (Extended Data Fig. 1c). None of the known stimuli, including anti-CD3, anti-CD28, anti-ICOS, interleukin (IL)-6 and IL-21, nor their combination, upregulated Ascl2 expression in T cells (Extended Data Fig. 1d). Ascl2 was previously shown to be a target of canonical Wnt signalling in intestinal stem cells⁵, and we also found that Ascl2 and CXCR5 but not Bcl6 expression in CD4⁺ T cells could be upregulated by TWS119 (ref. 16; Fig. 1f and Extended Data Fig. 1d, e) or other Wnt agonists (data not shown).

As a first step to examine the function of Ascl2 in T_{FH} cells, retroviral overexpression of Ascl2 was conducted in CD4⁺ T cells, leading to substantial induction of CXCR5 expression in over 30% of transduced cells, whereas overexpression of Bcl6, Batf or Maf in purified T cells did not (Fig. 2a and Extended Data Fig. 2a). Ascl2 overexpression increased Cxcr5 mRNA expression by ~60 fold (Fig. 2b), without affecting Bcl6, Prdm1, Batf, Sh2d1a, Cd40lg, Icos, Pdcld, Btla and Il21 expression (Fig. 2c). CXCR5 expression was equally induced by Ascl2 in wild-type, Bcl6^{−/−} and Batf^{−/−} CD4⁺ T cells *in vitro* (Fig. 2d). Thus, our findings suggest that Ascl2 is unique in its ability to induce CXCR5 protein expression in CD4⁺ T cells *in vitro*. CCR7 and PSGL1 (Selplg) as well as CD25 (Il2ra) and CD122 (Il2rb) expression were downregulated in Ascl2-overexpressing T cells (Fig. 2e and Extended Data Fig. 2b), probably accounting for increased follicular homing ability and decreased IL-2 signalling in T_{FH} cells^{14,15,17}. In addition, T_{H1}- and T_{H17}-related signature genes were strongly suppressed by Ascl2 (Extended Data Fig. 2c).

We then assayed the role of Ascl2 *in vivo* by transferring Ascl2-transduced OT-II cells. In Tcrb^{−/−} recipient mice, at day 2 after immunization with 4-hydroxy-3-nitrophenyl (NP)-ovalbumin (OVA) in CFA, neither CXCR5 nor Bcl6 expression were detectable in the vector-transduced control group, whereas Ascl2 overexpression strongly increased in CXCR5⁺Bcl6^{lo} cells (Fig. 2f, g). By contrast, ectopic expression of Bcl6 did not promote T_{FH}-cell generation at this time point (Extended Data Fig. 2d, e). At day 6 after immunization, Ascl2 overexpression induced a higher percentage of CXCR5^{hi}Bcl6^{hi} T_{FH} cells (Fig. 2f, g). Accordingly, germinal centre B cells and the total area of the germinal centre at day 8 in C57BL/6 mice receiving Ascl2-transduced T cells were significantly increased (Fig. 2h–j). Anti-NP immunoglobulin (Ig)M, IgA, IgG1 as well as IgG3 titres were increased in Tcrb^{−/−} mice, whereas

¹Tsinghua University School of Medicine, Beijing 100084, China. ²Department of Immunology, MD Anderson Cancer Center, Houston, Texas 77054, USA. ³Department of Lymphoma and Myeloma, MD Anderson Cancer Center, Houston, Texas 77054, USA. ⁴Institute for Systems Biology, Seattle, Washington 98103, USA. ⁵Laboratory of Immunology, National Eye Institute, NIH, Bethesda, Maryland 20892-1858, USA. ⁶Hubrecht Institute-KNAW and University Medical Center Utrecht, Uppsalalaan 8, 3584 CT Utrecht, the Netherlands. ⁷National Institute of Dental and Craniofacial Research, NIH, Bethesda, Maryland 20892-2190, USA. ⁸State Key Laboratory of Ophthalmology, Sun Yat-sen University, Guangzhou 510275, China. [†]Present addresses: College of Life Sciences, Wuhan University, Wuhan 430072, China (B.Z.); SomantiX B.V., Paduaalaan 8, 3584 CH Utrecht, the Netherlands (L.G.v.d.F.).

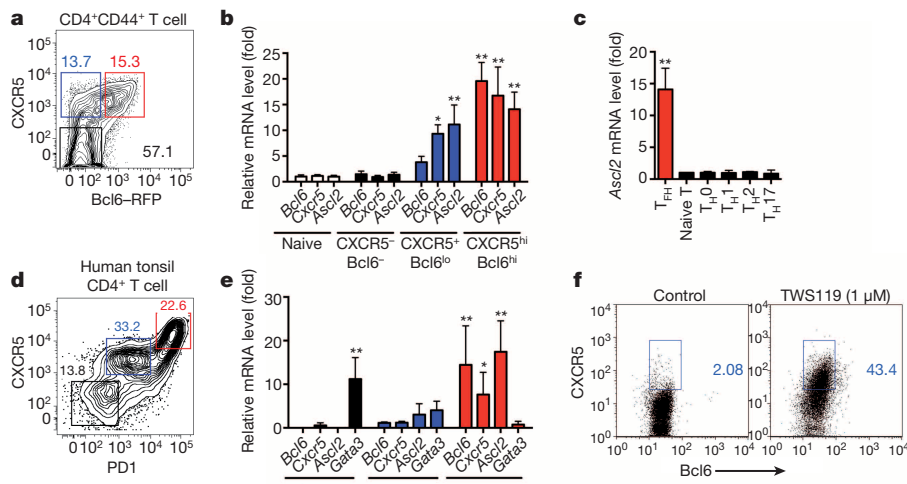


Figure 1 | Ascl2 is selectively expressed in both mouse and human T_{FH} cells. **a**, Three populations of CXCR5^{hi}Bcl6-RFP^{hi} (red), CXCR5⁺Bcl6-RFP^{lo} (blue) and CXCR5⁻Bcl6-RFP⁻ (black) cells were sorted from dLNs in Bcl6-RFP mice immunized with KLH emulsified in CFA subcutaneously. **b**, Ascl2, CXCR5 and Bcl6 transcriptional expression in sorted cells. **c**, Ascl2 mRNA expression among *in-vivo*-generated T_{FH}, naive, Th0, Th1, Th2 and Th17 cells by quantitative polymerase chain reaction with reverse transcription (RT-PCR). **d**, Flow cytometric analysis of human tonsil CD4⁺ T cells by CXCR5 and PD1

IgG2a and IgG2b were not affected by Ascl2-overexpressing T cells (Fig. 2k), consistent with IgG2a switching being primarily mediated by extrafollicular T cells¹⁸.

We next assessed whether Ascl2 could promote T-cell follicular homing *in vivo*. Ascl2-overexpressing OT-II cells preferentially accumulated in follicles (Fig. 2l), and even in the germinal centre (Fig. 2j), in comparison with control vector-infected T cells. Given that Bcl6 overexpression does not affect early T_{FH}-cell generation (Extended Data Fig. 2d, e) and T_{FH}-cell migration³, these observations collectively demonstrate that, by contrast with Bcl6, Ascl2 promotes T-cell migration to the follicles and the initiation of T_{FH}-cell development.

To investigate the mechanism of Ascl2-controlled T_{FH}-cell generation, we performed microarray analysis, and found that the expression of 293 genes was changed by more than twofold by Ascl2 overexpression. Cross-referencing the current data set of Ascl2 versus vector with our previous T_{FH}-cell versus non-T_{FH}-cell data set⁴ revealed that 85 of the 293 genes affected by Ascl2 were directly associated with T_{FH}-cell differentiation: 22 genes were upregulated and 63 genes were downregulated⁴ (Fig. 3a, b and Supplementary Table 1). The chemokine receptors CXCR5 and CXCR4, which are germinal centre T_{FH}-related receptors¹⁹, were at the top of the upregulated gene list, whereas Th1-related genes (*Il12rb1*, *Tbx21*, *Ifng* and *Gzmb*) and the Th17-related aryl hydrocarbon receptor (*Ahr*) gene were greatly suppressed by Ascl2 (Fig. 3a). When comparing Ascl2-RV-GFP-infected (GFP, green fluorescent protein; RV, retroviral vector) CXCR5⁺ T cells and CXCR5⁻ T cells with *in-vivo*-generated T_{FH} and non-T_{FH} cells⁴, we found that Ascl2-induced CXCR5⁺ T cells were more similar in gene expression to T_{FH} cells (Extended Data Fig. 2f, g), with ~350 genes commonly expressed in these cells (Extended Data Fig. 2h).

We further examined the effect of Ascl2 on Th1-, Th2- and Th17-cell differentiation. As shown in Extended Data Fig. 3a, overexpression of Ascl2 suppressed both Th1 and Th17 differentiation and induced CXCR5 expression. Ascl2 had no effect on TGF-β-induced Foxp3 expression but induced CXCR5⁺ regulatory T (T_{reg}) cells, suggesting that it may also be related to follicular T regulatory (T_{FR})-cell generation²⁰. Under Th2-polarized conditions, Ascl2 enhanced IL-4 expression, whereas it inhibited the expression of Gata3, IL-5 and IL-13 (Extended Data Fig. 3a–c), in agreement with recent studies that showed IL-4 but not

staining. **e**, The expression of Ascl2, Cxcr5, Bcl6 and Gata3 mRNA in sorted cells. **f**, CXCR5 expression in CD4⁺ T cells activated by anti-CD3/anti-CD28 in the presence of TWS119 (1 μM) (an inhibitor of glycogen synthase kinase 3β (GSK-3β)) for 3 days. All experiments were repeated at least three times with similar results. **b**, **c**, **e**, Bar graphs show the relative level of mRNA as mean ± standard deviation (s.d.), n = 3 per group. *P < 0.05, **P < 0.01, two-tailed t-test.

Gata3, IL-5 or IL-13 expression in T_{FH} cells²¹. Also, we observed that Ascl2 increased IL-4 but not IL-21 production *in vivo* (Extended Data Fig. 3d, e). Therefore, Ascl2 promotes T_{FH} gene expression and inhibits Th1-, Th2- and Th17-related gene expression.

We next assessed Ascl2 target genes by chromatin immunoprecipitation coupled with high-throughput sequencing (ChIP-seq). The analysis revealed a total of 10,028 Ascl2-binding peaks, among which 41% and 36% were enriched in intronic and intergenic regions, respectively (Fig. 3c). Only 20% of Ascl2-binding sites were located at promoter regions (Fig. 3c). Further comparison of global Ascl2-binding sites with the Ascl2-regulated gene list showed that 145 among 4,374 Ascl2-bound genes were transcriptionally regulated by Ascl2 (Fig. 3d).

As anticipated, analysis of the Ascl2-binding peaks identified an E-box protein-binding site (5'-CANNTG-3') as the consensus motif⁵ (Fig. 3e). Ascl2-binding sites were identified in groups of gene loci including receptor genes (*Cxcr5*, *Cxcr4*, *Ccr7*, *Selplg*, *Il2ra* and *Il2rb*) and inflammatory signature genes (*Ifng*, *Tbx21*, *Il2* and *Rorc*) (Fig. 3f), but not in some T_{FH}-related genes (*Bcl6*, *Prdm1*, *Pdcid1*, *Sh2d1a*, *Icos*, *Il21* and *Cd40lg*) (data not shown).

In particular, the *Cxcr5* locus was found to have multiple Ascl2-binding sites in the conserved non-coding sequence (CNS) regions (Fig. 3f, g). Moreover, these Ascl2-binding sites at the *Cxcr5* locus were confirmed in *in-vivo*-generated T_{FH} cells: two strong binding sites at intronic regions (CNS5 and CNS4-3), and three at distal promoter region (CNS1-1, CNS1 and CNS2) (Fig. 3f–h). Of note, the strongest Ascl2-binding peak was in the CNS5 region, which is consistent with the E47- (bHLH family member) binding site at the *Cxcr5* locus²² (Fig. 3f–h), implying a potentially redundant role of E2A in transcriptional regulation of the *Cxcr5* gene²³.

To examine the functional significance of Ascl2 binding in regulating CXCR5 expression, we introduced Id3, an inhibitor of the E-box protein²², into Ascl2-overexpressing OT-II cells by retroviral infection, and observed a substantial reduction in Ascl2-regulated CXCR5 expression (Extended Data Fig. 4a); this reduction was due to the inhibition of Ascl2 binding at the *Cxcr5* locus, as revealed by ChIP assay (Extended Data Fig. 4b). Additionally, a luciferase reporter assay showed that CNS5 and CNS1 were responsive to Ascl2 binding (Extended Data Fig. 4c, d). Together, these results provide evidence that Ascl2 is involved in the direct control of T_{FH}-cell programming.

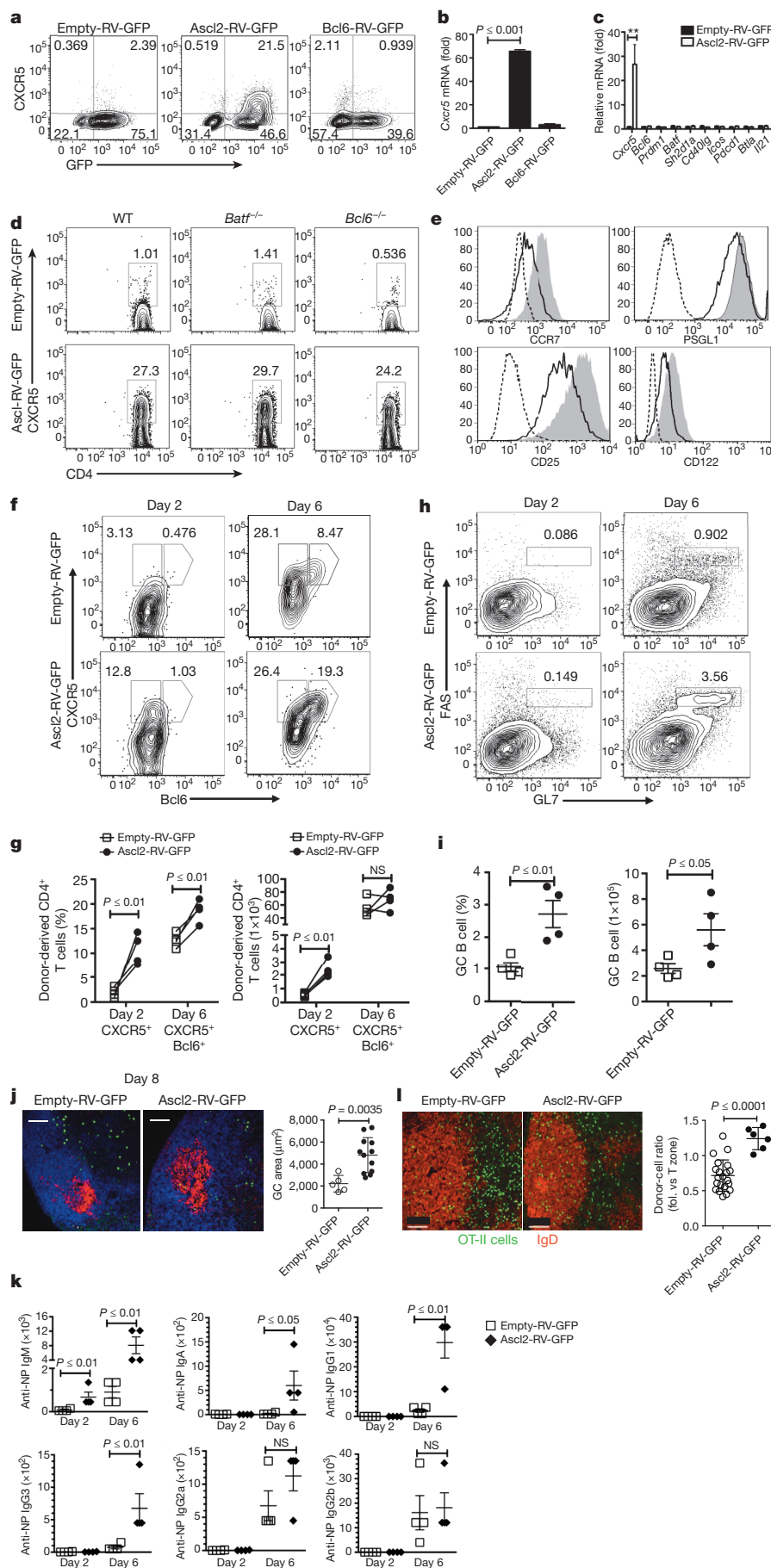


Figure 2 | Ascl2 expression induces the T_{FH} program. **a**, Flow cytometry analysis of surface CXCR5 expression from empty-RV-GFP, Ascl2-RV-GFP and Bcl6-RV-GFP retrovirus-infected T cells, respectively. **b**, Sorted GFP⁺ T cells were subjected to the measurement of Cxcr5 mRNA by quantitative RT-PCR. **c**, Measurement of gene expression, including Cxcr5, Bcl6, Prdm1, Batf, Sh2d1a, Cd40lg, Icos, Pdcdf, Btla and Il21. **d**, Surface CXCR5 expression in Ascl2-RV-GFP- and vector-virus-infected wild-type (WT), Bcl6^{-/-} and Batf^{-/-} T cells. **e**, CCR7, PSGL1, CD25 and CD122 expression by flow cytometry analysis. Dashed line, isotype; solid line, Ascl2-RV-GFP; shaded area, empty-RV-GFP. **f**, Ascl2-RV-GFP- or empty-RV-GFP-transduced GFP⁺ OT-II cells were transferred into naive *Tcrb*^{-/-} mice subsequently immunized with NP-OVA/CFA. **g**, At day 2 and day 6, flow cytometry analysis of donor cells was undertaken with staining for CXCR5 and Bcl6 ($n = 4$). **h**, Quantification of CXCR5⁺ and CXCR5⁺Bcl6⁺ donor-derived T cells. **i**, Germinal centre B cells (GL7^{hi}FAS^{hi}) in recipient mice ($n = 4$). **j**, Ascl2-RV-GFP- or empty-RV-GFP-transduced GFP⁺ OT-II were transferred into congenic mice. Four days later, each mouse was immunized subcutaneously with OVA (30 µg)/Alum/LPS. At day 8, dLNs were collected and subjected to histochemistry analysis. Green, GFP; red, Bcl6; blue, anti-IgD; scale bar, 100 µm, dot graph represents GC areas per slide view (some slides in Ascl2 group contain > 1 GC), displayed as mean ± s.d., control group ($n = 5$), Ascl2-RV-GFP group ($n = 12$). **k**, Titres of NP-specific antibodies in serum from mice on day 8 after immunization ($n = 4$). **l**, Distribution of Ascl2-RV-GFP- and vector-infected GFP⁺ OT-II donor cells in IgD⁺ B-cell follicles from dLNs in mice immunized with OVA/Alum/LPS for 4 days. Scale bar, 100 µm. Dot graph represents distribution with the ratio of donor cells in the B-cell follicle (fol.) versus the T zone, displayed as mean ± s.d. Empty-RV-GFP, $n = 21$; Ascl2-RV-GFP, $n = 15$. All experiments were repeated at least two times with similar results. **b**, **c**, **g**, **i**, **j**–**l**, Graphs show data as mean ± s.d., two-tailed *t*-test. NS, not significant.

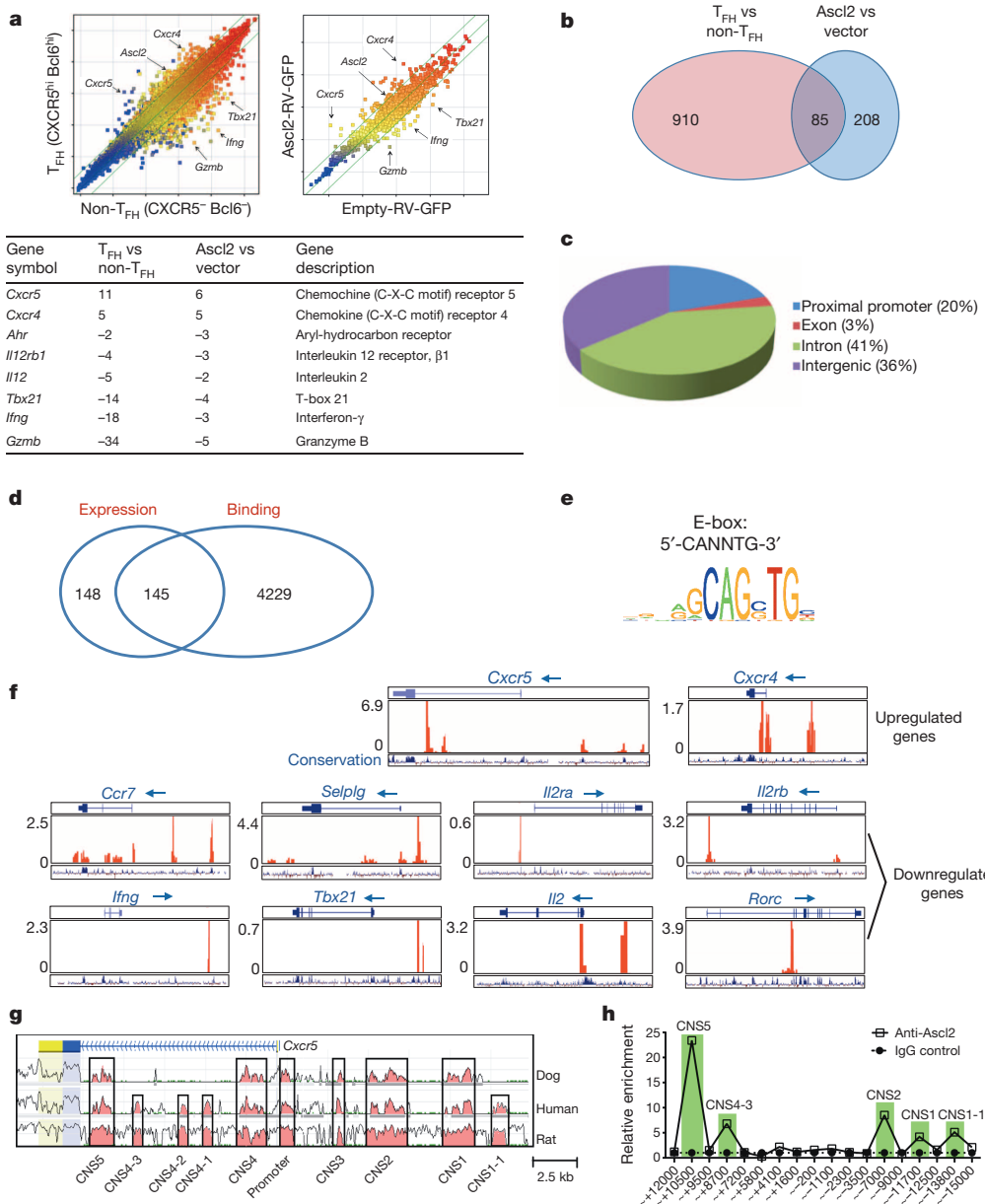


Figure 3 | Ascl2-dependent transcriptional regulation of T_{FH}-related genes. **a**, Scatterplot of the average signal of T_{FH} versus non-T_{FH} cells, and Ascl2-RV-GFP⁺ versus empty-RV-GFP⁺ T-cell gene expression microarray data. The green line indicates gene expression change by a factor of 2; data normalized from two replicates are shown; $n = 2$. Genes with the most transcriptional changes are listed. **b**, Venn diagram of genes regulated by Ascl2 and T_{FH}-related genes. **c**, Distribution of Ascl2 ChIP-seq peaks in Ascl2-overexpressed CD4⁺ T

As Maf¹⁰, Batf^{1,12} and IRF4 (ref. 13) are required in T_{FH}-cell differentiation, we compared genome-wide occupancy of these transcriptional factors, and found that Ascl2-bound genes hardly correlated with those bound by Maf (Extended Data Fig. 5a). For instance, IL-21 is directly regulated by Maf²⁴, but not by Ascl2 (Extended Data Fig. 5b). Additionally, there was no binding site for Maf at the Ascl2 locus (data not shown), or vice versa (Extended Data Fig. 5b), suggesting that Ascl2 and Maf are functionally independent in T_{FH} cells. A large proportion of Ascl2 occupancy colocalized with Batf/IRF4-binding sites (Extended Data Fig. 5c), including at the CNS of gene loci including Cxcr5, Cxcr4, Ccr7, Selplg, Il2, Il2ra and Il2rb (Extended Data Fig. 5d), but not at Bcl6, Prdm1 and Maf (Extended Data Fig. 5b). Interestingly, Batf/IRF4 and Ascl2 peaks were found to be independently localized in T_{H1}, T_{H2} and T_{H17} signature genes (Extended Data Fig. 5e–g), indicating that Batf/IRF4 acts downstream of the T-cell antigen receptor

cells. **d**, Venn diagram of genes regulated by Ascl2 and Ascl2-bound genes. **e**, The Ascl2-binding site is identical to the E-box-binding motif. **f**, Ascl2-binding peaks located at gene loci including Cxcr5, Cxcr4, Ccr7, Selplg, Il2ra, Il2rb, Ifng, Tbx21, Il2 and Rorc. **g**, Comparison of the mouse Cxcr5 genomic sequence with that of dog, human and rat. Red regions denote CNS region. **h**, Ascl2-binding sites at the Cxcr5 locus in *in-vivo*-generated T_{FH} cells as determined by ChIP-qPCR (primers are listed in Supplementary Table 2).

(TCR) in activation of effector programs²⁵, whereas Ascl2 mediates suppression. These data strongly support Ascl2 acting as a specific regulator in T_{FH} cells.

T_{FH} cells provide important help to B cells in the induction of efficient anti-virus antibodies during viral infection^{6,26}. To address the functional roles of Ascl2, we generated Ascl2^{fl/fl}/CD4-Cre mice, in which T cells were developmentally intact (data not shown), and assessed the requirement of Ascl2 in T_{FH}-cell development *in vivo* with influenza virus infection. After intranasal infection, Ascl2^{fl/fl}/CD4-Cre mice developed gradual body weight loss from day 3 to day 9, whereas control littermate mice recovered after day 8 (Extended Data Fig. 6a). At day 9 post-infection (d.p.i.), viral haemagglutinin (HA) mRNA expression in the lungs of Ascl2^{fl/fl}/CD4-Cre mice was over fivefold higher than that in control mice (Extended Data Fig. 6b), whereas CXCR5⁺Bcl6⁺ T_{FH} cells in lung draining lymph nodes (dLNs) had

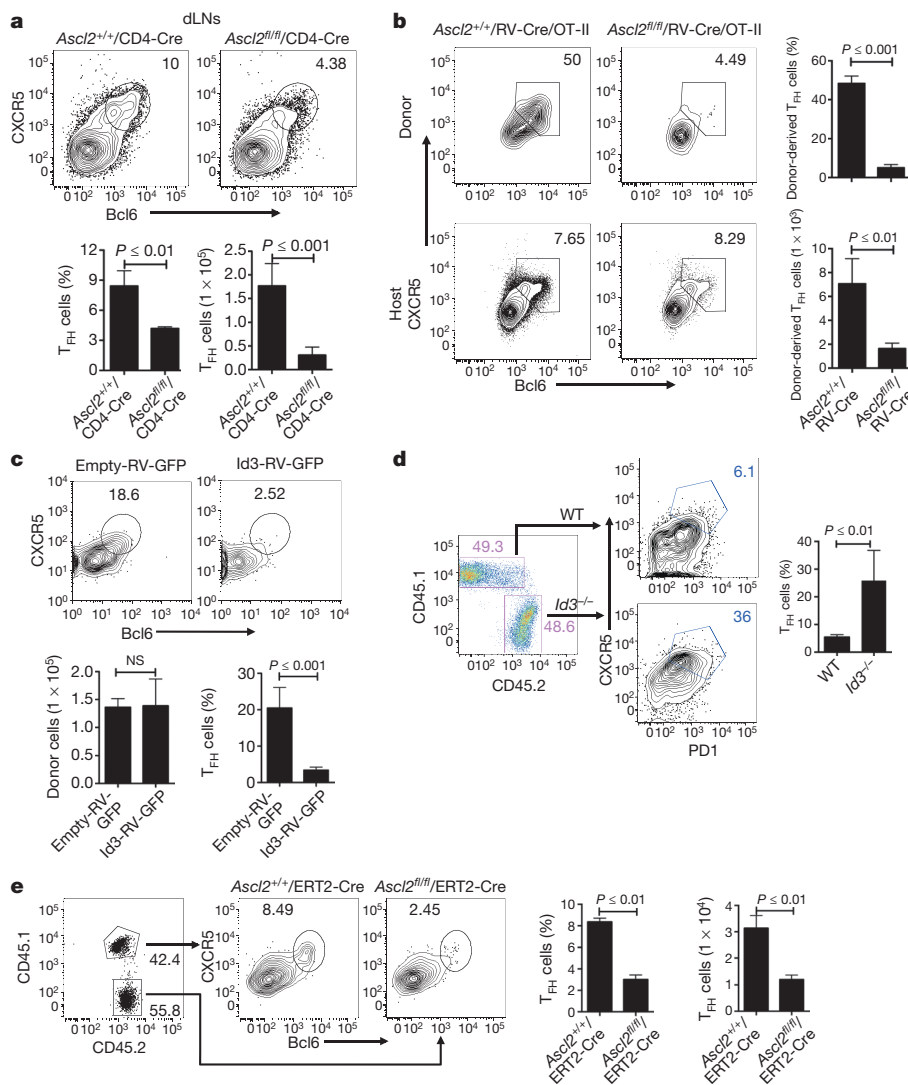


Figure 4 | Loss of Ascl2 in peripheral CD4⁺ T cells inhibits T_{FH} differentiation. **a**, T_{FH} cells (CXCR5^{hi}Bcl6^{hi}) in mediastinal LNs from Ascl2^{fl/fl}/CD4-Cre and Ascl2^{+/+}/CD4-Cre mice that had received a sublethal dose of influenza virus A/Puerto Rico/8 (H1N1) intranasally 9 days before ($n = 5$). **b**, Flow cytometry analysis of donor cells or host cells in mice receiving Cre-RV-GFP retrovirus-infected Ascl2^{fl/fl}/OT-II or Ascl2^{+/+}/OT-II GFP⁺ cells and subcutaneous 5-day immunization with OVA/CFA ($n = 3$). **c**, Flow cytometry analysis of donor-derived T_{FH} cells in mice that had received Id3-RV-GFP or control viral-vector-transduced OT-II cells and subcutaneous OVA/CFA immunization ($n = 3$). **d**, Flow cytometry analysis of donor-derived T_{FH} cells in *Rag*^{-/-} mice receiving equal numbers of naïve *Id3*^{-/-} and wild-type (WT) CD4⁺ T cells and subcutaneous KLH/CFA immunization for 7 days ($n = 5$). **e**, Analysis and quantification of T_{FH} cells in chimaeric mice reconstituted with equal numbers of Ascl2^{fl/fl}/ERT2-Cre and Ascl2^{+/+}/ERT2-Cre bone marrow cells after 5-day tamoxifen treatment and 7-day KLH/CFA immunization ($n = 4$). All data are representative of three independent experiments. Bar graphs show mean \pm s.d., two-tailed *t*-test. NS, not significant.

decreased by over 50%, there was a \sim 3–4-fold decrease in total cell numbers in the absence of Ascl2 (Fig. 4a), probably accounting for a severe reduction in germinal centre B-cell formation and anti-viral IgG production (Extended Data Fig. 6c, d). Also, T_{FH}-cell and germinal centre B-cell development in the spleen was reduced in Ascl2^{fl/fl}/CD4-Cre mice (Extended Data Fig. 6e, f). No difference was found between CD8⁺ T-cell populations in the lung, bronchoalveolar lavage fluid (BALF), spleen and dLNs in Ascl2^{fl/fl}/CD4-Cre mice and control mice (Extended Data Fig. 6g), although CD8⁺ T-cell activation in the dLNs of Ascl2^{fl/fl}/CD4-Cre mice was slightly enhanced (Extended Data Fig. 6h). Moreover, we applied the same assay to tamoxifen-treated mixed bone marrow chimaeric mice receiving both Ascl2^{fl/fl}/ERT2-Cre and Ascl2^{+/+}/ERT2-Cre bone marrow cells, and found a \sim 50% decrease in T_{FH} cells in the Ascl2^{fl/fl}/ERT2-Cre counterpart, whereas no defect was found in Ascl2-ablated CD8⁺ T cells (Extended Data Fig. 6i, j).

Because Ascl2 can form heterodimers with three other bHLH family members, including E2-2 (also known as TCF4), E47 (also known as TCF3) and HEB (also known as TCF12) in human cells^{5,23}, this suggests that the partial defect in T_{FH}-cell differentiation in Ascl2^{fl/fl}/CD4-Cre mice might be caused by compensation from other bHLH members. Indeed, T_{FH} cells and germinal centre responses were normal in Ascl2^{fl/fl}/CD4-Cre mice after immunization with KLH in CFA (data not shown). A substantial enhancement of E47 expression was noticed in naïve T, T_{FH} and even non-T_{FH} cells from Ascl2^{fl/fl}/CD4-Cre mice compared with control mice (Extended Data Fig. 7a), and expression of E47 also

increased CXCR5 expression in CD4⁺ T cells (Extended Data Fig. 7b), consistent with a recent report that increased E47 activity in *Id3*^{-/-} mice is associated with increased T_{FH}-like cells²². Furthermore, we examined T-cell maturation and T_{FH}-cell differentiation in chimaeric mice receiving both Ascl2^{fl/fl}/CD4-Cre and Ascl2^{+/+}/CD4-Cre, or only Ascl2^{fl/fl}/CD4-Cre bone marrow cells. As shown in Extended Data Fig. 7c, d, in chimaeric mice, Ascl2 deficiency reduced TCR-β^{hi}CD69^{lo} mature T cells, whereas mice receiving only Ascl2^{fl/fl}/CD4-Cre cells had fewer defects in T-cell maturation. Accordingly, after immunization with KLH/CFA, T_{FH}-cell generation was inhibited in the Ascl2^{fl/fl}/CD4-Cre counterpart from mixed chimaeric mice (Extended Data Fig. 7e–g). These data suggest that Ascl2 deletion at an early developmental stage induces compensatory mechanisms to allow T-cell maturation.

To overcome the inducible compensation mechanism, we deleted the Ascl2 gene acutely using a Cre-expressing retrovirus and examined T_{FH}-cell differentiation. As shown in Fig. 4b, Ascl2 deficiency in this case resulted in an absolute impairment in T_{FH} development *in vivo*. By contrast, Bcl6-deficient OT-II cells showed intact CXCR5 expression and homing ability at day 3 after immunization (Extended Data Fig. 8a–e). Moreover, Id3 overexpression impaired T_{FH}-cell generation and germinal centre responses (Fig. 4c and Extended Data Fig. 9a–c). Conversely, Id3 deficiency enhanced the T_{FH}-cell population (Fig. 4d). Together with the observation that Bcl6 overexpression could not rescue Id3-induced T_{FH} blockage (Extended Data Fig. 9d), Ascl2 seems to have an earlier function than Bcl6 in T_{FH}-cell development.

To confirm this, we examined T_{FH}-cell differentiation in either mixed chimaeric mice receiving equal numbers of *Ascl2*^{fl/fl}/ETR2-Cre and *Ascl2*^{+/+}/ETR2-Cre bone marrow cells (Fig. 4e), or intact *Ascl2*^{fl/fl}/ETR2-Cre mice (data not shown). After tamoxifen treatment and KLH/CFA immunization, *Ascl2* deletion inhibited T_{FH}-cell differentiation and germinal centre response *in vivo* (Fig. 4e and data not shown). Therefore, these data verify that *Ascl2* is intrinsically necessary for T_{FH}-cell differentiation.

We have identified a new player—the *Ascl2* transcription factor—that is crucial for T_{FH}-cell development and function. On the one hand, similar to Bcl6, *Ascl2* acts as a novel suppressor of T_{H1}, T_{H2}- and T_{H17}-cell differentiation. On the other hand, *Ascl2* uniquely regulates T_{FH}-cell migration and development by increasing CXCR5 and CXCR4 expression, and suppressing CCR7 and PSGL1 expression, and IL-2 signalling. Our data indicate that *Ascl2* and Bcl6 act to program T_{FH}-cell generation. Activated T cells by antigen-presenting cells gain *Ascl2* expression, which allows their migration towards B-cell follicles. At the T-B border, cognate B cells provide another signal for precursor T_{FH} cells to increase Bcl6 expression, which completes T_{FH} polarization and germinal centre formation. Therefore, Id3 and *Ascl2* may serve as an early checkpoint during T_{FH}-cell development in promoting appropriate antibody responses to infection while keeping autoimmune diseases in check (Extended Data Fig. 10). Further investigation into this axis may offer new ways to modulate antibody responses in infection and autoimmunity.

METHODS SUMMARY

Mice, immunization and infection. *Ascl2*^{fl/fl} mice were generated previously⁵ and had been backcrossed with C57BL/6 for at least six generations. Mice were immunized with antigens emulsified in CFA subcutaneously (100 µl each mouse). Influenza virus A/Puerto Rico/8 (PR8, H1N1) was purchased from Charles River Laboratories. Mice were anaesthetized by intraperitoneal injection with ketamine and infected intranasally with a dose of PR8 influenza virus²⁷ lethal to 50% of animals tested (LD₅₀) of 0.5.

ChIP-seq. ChIP-seq was performed as described previously²⁸. The DNA fragments were sequenced with an Illumina 1G Analyzer at the Institute for System Biology. The output of the Solexa Analysis Pipeline was converted to browser-extensible data (BED) files, and the data were viewed in the UCSC genome browser.

Statistics. Unless specifically indicated, comparison between different groups was conducted with Student's *t*-tests. All *P* values below 0.05 were considered significant. Statistical analysis was performed with Graphpad Prism 6.

Online Content Any additional Methods, Extended Data display items and Source Data are available in the online version of the paper; references unique to these sections appear only in the online paper.

Received 9 April; accepted 26 November 2013.

Published online 19 January; corrected online 26 March 2014 (see full-text HTML version for details).

- Liu, X., Nurieva, R. I. & Dong, C. Transcriptional regulation of follicular T-helper (Tfh) cells. *Immunol. Rev.* **252**, 139–145 (2013).
- Vinuesa, C. G. & Cyster, J. G. How T cells earn the follicular rite of passage. *Immunity* **35**, 671–680 (2011).
- Xu, H. et al. Follicular T-helper cell recruitment governed by bystander B cells and ICOS-driven motility. *Nature* **496**, 523–527 (2013).
- Liu, X. et al. Bcl6 expression specifies the T follicular helper cell program *in vivo*. *J. Exp. Med.* **209**, 1841–1852 (2012).
- van der Flier, L. G. et al. Transcription factor achaete scute-like 2 controls intestinal stem cell fate. *Cell* **136**, 903–912 (2009).
- Crotty, S. Follicular helper CD4 T cells (T_{FH}). *Annu. Rev. Immunol.* **29**, 621–663 (2011).
- Johnston, R. J. et al. Bcl6 and Blimp-1 are reciprocal and antagonistic regulators of T follicular helper cell differentiation. *Science* **325**, 1006–1010 (2009).

- Nurieva, R. I. et al. Bcl6 mediates the development of T follicular helper cells. *Science* **325**, 1001–1005 (2009).
- Yu, D. et al. The transcriptional repressor Bcl-6 directs T follicular helper cell lineage commitment. *Immunity* **31**, 457–468 (2009).
- Bauquet, A. T. et al. The costimulatory molecule ICOS regulates the expression of c-Maf and IL-21 in the development of follicular T helper cells and T_H-17 cells. *Nature Immunol.* **10**, 167–175 (2009).
- Betz, B. C. et al. Batf coordinates multiple aspects of B and T cell function required for normal antibody responses. *J. Exp. Med.* **207**, 933–942 (2010).
- Ise, W. et al. The transcription factor BATF controls the global regulators of class-switch recombination in both B cells and T cells. *Nature Immunol.* **12**, 536–543 (2011).
- Kwon, H. et al. Analysis of interleukin-21-induced *Prdm1* gene regulation reveals functional cooperation of STAT3 and IRF4 transcription factors. *Immunity* **31**, 941–952 (2009).
- Johnston, R. J., Choi, Y. S., Diamond, J. A., Yang, J. A. & Crotty, S. STAT5 is a potent negative regulator of T_{FH} cell differentiation. *J. Exp. Med.* **209**, 243–250 (2012).
- Nurieva, R. I. et al. STAT5 protein negatively regulates T follicular helper (Tfh) cell generation and function. *J. Biol. Chem.* **287**, 11234–11239 (2012).
- Gattinoni, L. et al. Wnt signalling arrests effector T cell differentiation and generates CD8⁺ memory stem cells. *Nature Med.* **15**, 808–813 (2009).
- Ballesteros-Tato, A. et al. Interleukin-2 inhibits germinal center formation by limiting T follicular helper cell differentiation. *Immunity* **36**, 847–856 (2012).
- Lee, S. K. et al. B cell priming for extrafollicular antibody responses requires Bcl-6 expression by T cells. *J. Exp. Med.* **208**, 1377–1388 (2011).
- Allen, C. D. et al. Germinal center dark and light zone organization is mediated by CXCR4 and CXCR5. *Nature Immunol.* **5**, 943–952 (2004).
- Chung, Y. et al. Follicular regulatory T cells expressing Foxp3 and Bcl-6 suppress germinal center reactions. *Nature Med.* **17**, 983–988 (2011).
- Liang, H. E. et al. Divergent expression patterns of IL-4 and IL-13 define unique functions in allergic immunity. *Nature Immunol.* **13**, 58–66 (2012).
- Miyazaki, M. et al. The opposing roles of the transcription factor E2A and its antagonist Id3 that orchestrate and enforce the naive fate of T cells. *Nature Immunol.* **12**, 992–1001 (2011).
- Murre, C. et al. Interactions between heterologous helix-loop-helix proteins generate complexes that bind specifically to a common DNA sequence. *Cell* **58**, 537–544 (1989).
- Hiramatsu, Y. et al. c-Maf activates the promoter and enhancer of the IL-21 gene, and TGF-β inhibits c-Maf-induced IL-21 production in CD4⁺ T cells. *J. Leukoc. Biol.* **87**, 703–712 (2010).
- Ciofani, M. et al. A validated regulatory network for Th17 cell specification. *Cell* **151**, 289–303 (2012).
- Yoo, J. K., Fish, E. N. & Braciale, T. J. LAPCs promote follicular helper T cell differentiation of Ag-primed CD4⁺ T cells during respiratory virus infection. *J. Exp. Med.* **209**, 1853–1867 (2012).
- Zhang, Y. et al. MKP-1 is necessary for T cell activation and function. *J. Biol. Chem.* **284**, 30815–30824 (2009).
- Wei, G. et al. Global mapping of H3K4me3 and H3K27me3 reveals specificity and plasticity in lineage fate determination of differentiating CD4⁺ T cells. *Immunity* **30**, 155–167 (2009).

Supplementary Information is available in the online version of the paper.

Acknowledgements We thank J. A. Whitsett and J. P. Bridges at the University of Cincinnati for their provision of *Ascl2* conditional knockout mice, D. Yi for help with ChIP-seq and microarray analysis, R. Dalla-Favera for *Bcl6*^{−/−} mice, H. Hu for histochemistry staining, and the Dong laboratory members for their help. This work was supported in part by a grant from the National Institutes of Health (NIH; AI106654 to C.D.), an intramural research program (NIDCR to W.C. and H.N.), an NIH Lymphoma SPORE (to X.L.), an Odyssey fellowship from the MD Anderson Cancer Center (to X.L. and B.Z.), Chinese Ministry of Science and Technology '973' program grants (2014CB542501 and 2012CB910402), and a National Natural Science Foundation of China grant (81361120397 to H.Q.).

Author Contributions X.L. designed and performed the experiments, and wrote the manuscript; X.C. and H.Q. performed histochemistry in Fig. 2j, I and Extended Data Fig. 9a, b, and B.Z., A.W., X.W., R.I.N., F.C. and S.S.N. contributed to the performance of the other experiments; X.Y., P.C., Q.T. and L.W. performed microarray, ChIP product sequencing and data analysis; L.G.v.d.F., H.N., W.C. and H.C. provided important mouse strains; and C.D. designed and directed the research.

Author Information Microarray and ChIP-seq data have been deposited at GenBank under accession GSE52840. Reprints and permissions information is available at www.nature.com/reprints. The authors declare no competing financial interests. Readers are welcome to comment on the online version of the paper. Correspondence and requests for materials should be addressed to C.D. (cdonglab@hotmail.com) or X.L. (xindongliu@hotmail.com).

METHODS

Mice. Mice were housed in specific pathogen-free animal facilities at the MD Anderson Cancer Center and Tsinghua University, and were used according to protocols approved by the Institutional Animal Care and Use Committee. Six to eight week old mice were used for all experiments, and were randomly allocated into treatment groups. C57BL/6 mice were from the National Cancer Institute. ETR2-Cre, CD4-Cre, OT-II, B6S JL, *Tcrb*^{-/-}, *Rag1*^{-/-} and *Batf*^{-/-} mice were from Jackson Laboratories. *Stat5*^{-/-} (ref. 15), *Id3*^{-/-} (ref. 29), *Bcl6*-RFP (ref. 4) and *Bcl6*^{-/-} (ref. 8) mice were previously described.

The *Ascl2*^{fl/fl} mice were generated previously and had been backcrossed with C57BL/6 for at least six generations⁵. *Ascl2*^{fl/fl} mice were bred with CD4-Cre mice to generate *Ascl2*^{fl/fl}/CD4-Cre and *Ascl2*^{+/+}/CD4-Cre control mice. *Ascl2*^{fl/fl} mice were crossed with ETR2-Cre mice to generate *Ascl2*^{fl/fl}/ETR2-Cre and *Ascl2*^{+/+}/ETR2-Cre control mice. Ascl2 deletion in *Ascl2*^{fl/fl}/ETR2-Cre cells was achieved by administering 200 µl tamoxifen (5 mg ml⁻¹) in sunflower seed oil subcutaneously or intraperitoneally (i.p.) every other day for a total of 5 days.

KLH, NP-KLH, OVA and NP-OVA Immunization. Mice and their wild-type controls (6–8 weeks old; three per group) were immunized with antigen (0.5 mg ml⁻¹) emulsified in CFA (0.5 mg ml⁻¹) subcutaneously (100 µl per mouse). After immunization, these mice were killed and analysed individually. Germinal centre B cells were determined by staining with FITC-labelled anti-GL7, PE-labelled anti-FAS and PerCP-labelled anti-B220 monoclonal antibody (Pharmingen). T_{FH} cells were determined by staining with PerCP-labelled anti-CD4 monoclonal antibody and biotinylated anti-CXCR5 monoclonal antibody (Pharmingen), followed by APC-labelled streptavidin (Jackson ImmunoResearch Laboratories) and surface staining by PE-labelled anti-PD1 monoclonal antibody or intracellular staining by PE-labelled anti-Bcl6 monoclonal antibody (Pharmingen). Sera from immunized mice were collected, and antigen-specific IgM, IgA, IgG1, IgG3, IgG2a and IgG2b antibodies were measured by using ELISA. Briefly, isotype-specific antibodies to NP were measured in plates coated with NP₄-BSA using the SBA Clonotyping System (Southern Biotech). Titres were presented as the maximum serum dilution exceeding 1.5-fold above the average background. KLH- or OVA-specific titres were measured in a threefold serial dilution onto plates pre-coated with 100 µg ml⁻¹ KLH or OVA.

Influenza virus infection. Influenza virus A/Puerto Rico/8 (PR8, H1N1) was purchased from Charles River Laboratories. Six to eight week old *Ascl2*^{fl/fl}/CD4-Cre mice (3–5 mice per group) were anaesthetized by i.p. injection with ketamine and infected intranasally with a dose of PR8 influenza virus²⁷ lethal to 50% of animals tested (LD₅₀) of 0.5. Mice were monitored daily, and weight loss was recorded. To analyse influenza-virus-specific germinal centre responses, T_{FH} and germinal centre B cells from lung mediastinal lymph nodes and spleens were analysed by flow cytometry. BALF and sera were collected from virus-infected mice on 9 d.p.i. Virus-specific IgG antibodies were measured using ELISA. Briefly, serum samples were added in a threefold serial dilution onto plates pre-coated with heat-inactivated virus. Bound antibodies were detected by the incubation of horseradish-peroxidase-conjugated anti-mouse total IgG (1:10,000; Southern Biotech) antibodies. Lung viral titre was monitored by examining influenza virus HA and neuraminidase (NA) gene expression using real-time RT-PCR as previously described²⁷.

Retroviral transduction and T-cell differentiation. Naive CD4⁺CD25⁻CD44^{low}CD62L^{high} T cells from *Ascl2*^{fl/fl}/OT-II, OT-II or C57BL/6 mice were FACS sorted and activated with plate-bound anti-CD3e (clone, 2C11) and anti-CD28 (clone, 37.51) under neutral conditions. Thirty-six hours after activation, cells were infected by retroviruses Ascl2-RV-GFP, Bcl6-RV-GFP, Batf-RV-GFP, Maf-RV-GFP, Id3-RV-GFP, Cre-RV-GFP, E47-RV-CFP (a gift from Y. Zhuang) or control empty vector (empty-RV-GFP or empty-RV-CFP). One day after infection, GFP cells were FACS sorted for adoptive transfer, or followed by re-stimulation with pre-coated

anti-CD3e. Also, virus-infected cells were polarized under T_{H1} (IL-12, anti-IL-4), T_{H2} (IL-4, anti-IFN-γ), T_{H17} (TGF-β, IL-6, IL-23, anti-IL-4, anti-IFN-γ) and T_{Reg} (TGF-β) conditions. Four days after culture, cells were re-stimulated with PMA and ionomycin in the presence of Golgi-stop for 4 h, after which IFN-γ-, IL-4/IL-5/IL-13-, IL-17- and Foxp3-expressing cells were analysed using intracellular staining. Cytokines including IL-4, IL-5 and IL-13 from Ascl2-RV-GFP-infected T_{H2} cells were measured by ELISA. Cell transfer numbers for different cells were as follows: 1 × 10⁵ for GFP⁺ T cells; 8 × 10⁶ for bone marrow cells.

Mixed chimaeric bone marrow mice. To generate mixed bone marrow chimaeras, T-cell-depleted bone marrow cells were obtained from *Ascl2*^{fl/fl}/CD4-Cre or *Ascl2*^{fl/fl}/ERT2-Cre and their respective congenic wild-type (CD45.1⁺CD45.2⁺) mice, and mixed at a ratio of 1:1 before being transferred into irradiated *Rag1*^{-/-} (750 rad) mice. Six to eight weeks later, the reconstituted mice were subject to immunization and analysis as described earlier.

Microarray and ChIP-seq. Total cellular RNA was extracted from cells transduced with vector or Ascl2-expressing retrovirus that were purified by their expression of GFP marker with TRIzol reagent (Invitrogen). DNA microarray labelling and analysis were performed by microarray core at the Institute for System Biology. Approximately 10 µg of RNA was labelled and hybridized to GeneChip Mouse Gene 1.0 ST Array (Affymetrix) according to the manufacturer's protocols. Expression values were defined with GeneChip Operating Software (GCOS) software.

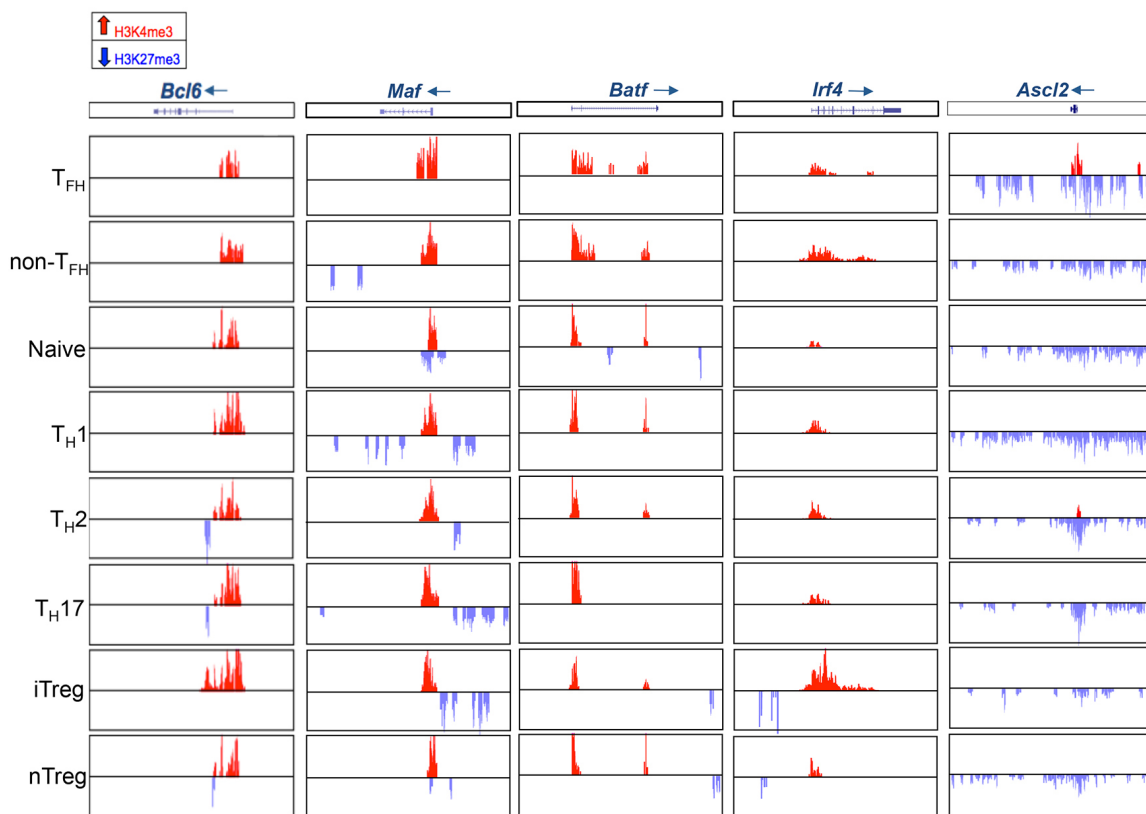
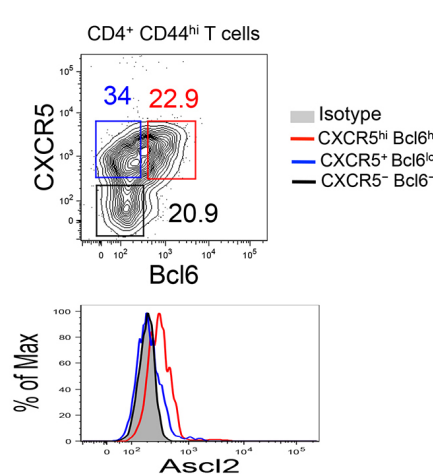
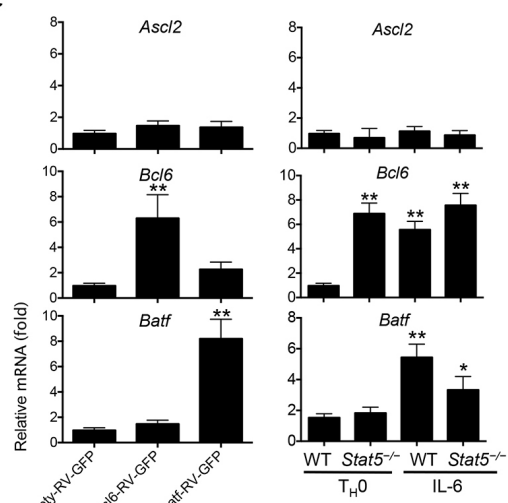
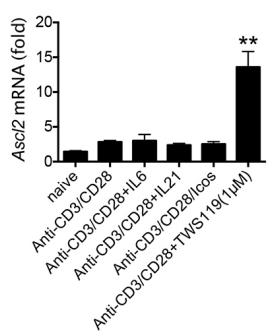
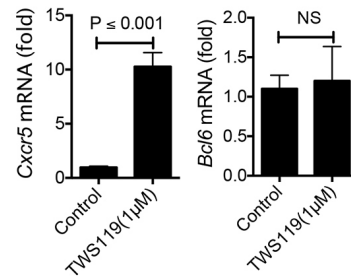
ChIP-seq was performed as described previously²⁸. Briefly, sorted T cells were fixed by 1% paraformaldehyde, and this was followed by digestion with Mnase cocktail (Active motif). Chromatin from 5 × 10⁶ cells was used for each ChIP experiment. Antibodies against H3K4me3 (catalogue no. 07-473, Millipore), H3K27me3 (catalogue no. 07-449, Millipore) and Ascl2 monoclonal antibody (clone 7E2, Millipore) were used. The pull-down DNA fragments were blunt-end ligated with Solexa adaptors, and amplified for sequencing. The DNA fragments were sequenced with an Illumina 1G Analyzer at the Institute for System Biology. The output of the Solexa Analysis Pipeline was converted to browser-extensible data (BED) files, and the data were viewed in the UCSC genome browser.

Immunohistochemistry. The protocol for immunohistochemical staining was as described previously³⁰. Staining reagents included biotinylated PNA (Vector), AlexaFluor 647 anti-B220, biotinylated anti-IgD, AlexaFluor 488 anti-CD45.2 (Biologend), and streptavidin AlexaFluor 568 (Invitrogen). All stained slides were mounted with ProlongGold antifade reagents (Invitrogen) and examined with an Olympus FV1000 confocal system.

Real-time RT-PCR analysis. Reactive tonsils were obtained from children undergoing elective tonsillectomy after informed consent in a protocol approved by the Institutional Review Board²⁰. Total RNA was extracted with Trizol reagent (Invitrogen). Oligonucleotide (dT) and MMLV reverse transcriptase (Invitrogen) were used to generate cDNA. Gene expressions were examined using the iQ SYBR real-time kit (Bio-Rad Laboratories). The data were normalized to a reference gene: β-actin. The primer pairs for real time RT-PCR analysis of Bcl6, Batf, CXCR5, IL-21, IL-4, Gata3, IFN-γ, T-bet, IL-17A and RORγ were previously described⁴. The primer pair for detection of mouse Ascl2 was: forward, 5'-CGCTGCCAGAC TCATGCC-3'; reverse, 5'-GCTTTACGCGGTTGCGCTCG-3'.

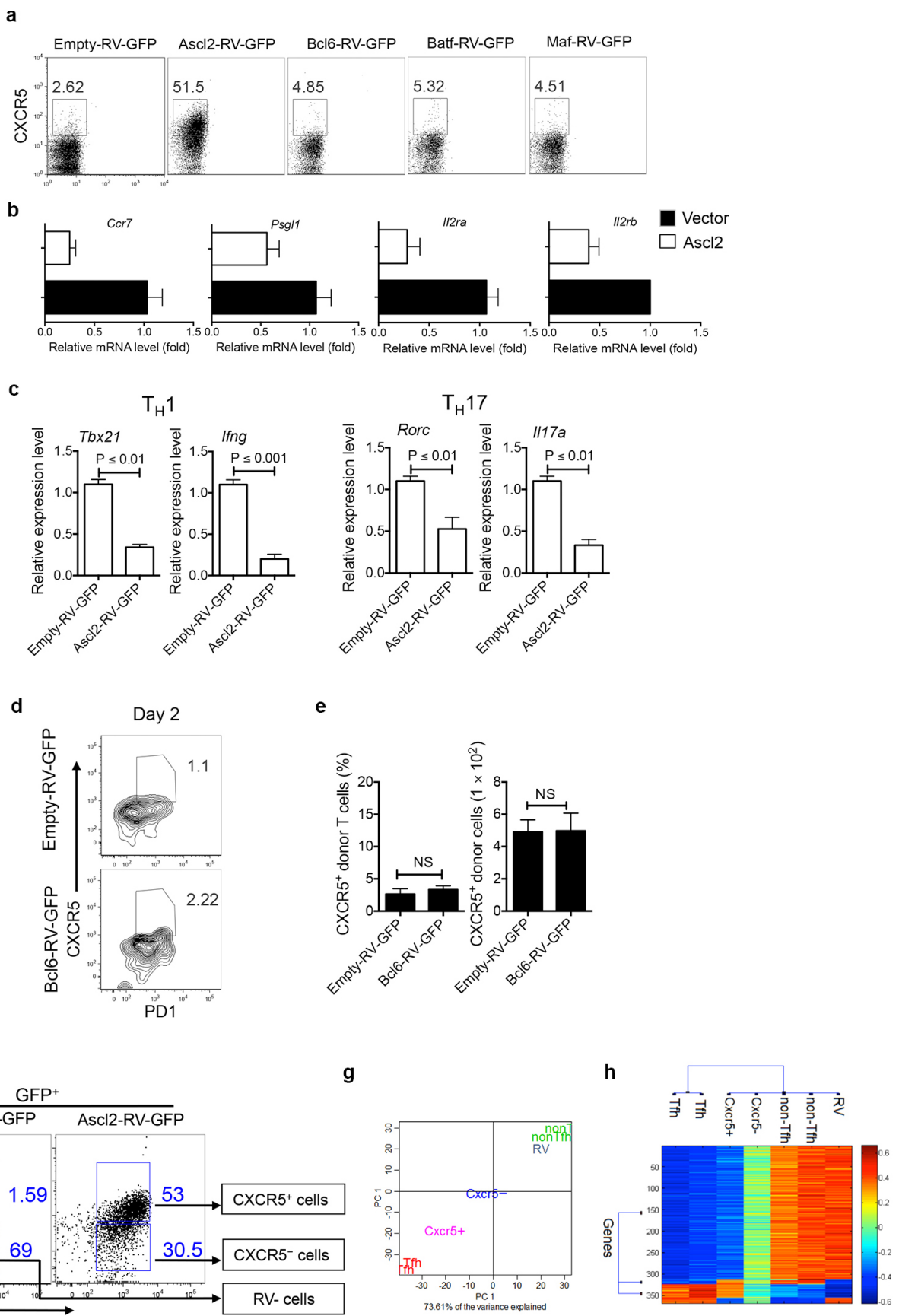
Statistics. Unless specifically indicated otherwise, comparison between two different groups was done with unpaired two-tailed Student's *t*-tests or two-way analysis of variance (ANOVA). All *P* values below 0.05 were considered significant. Statistical analysis was performed with Graphpad Prism 6.

29. Maruyama, T. et al. Control of the differentiation of regulatory T cells and T_{H17} cells by the DNA-binding inhibitor Id3. *Nature Immunol.* **12**, 86–95 (2011).
30. Qi, H., Cannons, J. L., Klauschen, F., Schwartzberg, P. L. & Germain, R. N. SAP-controlled T–B cell interactions underlie germinal centre formation. *Nature* **455**, 764–769 (2008).

a**b****c****d****e**

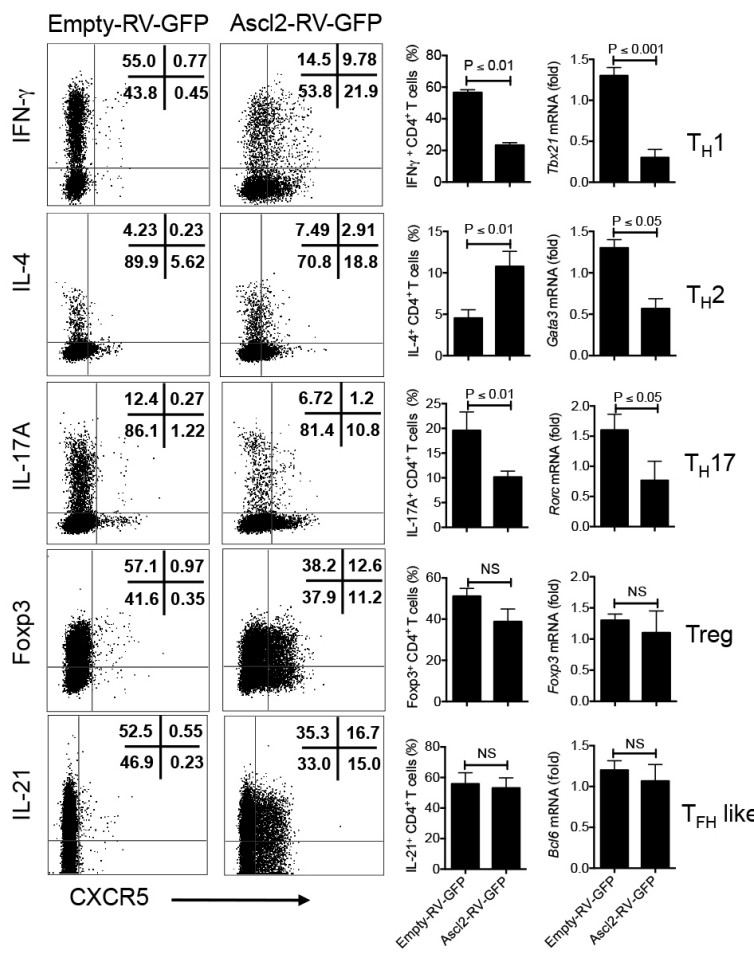
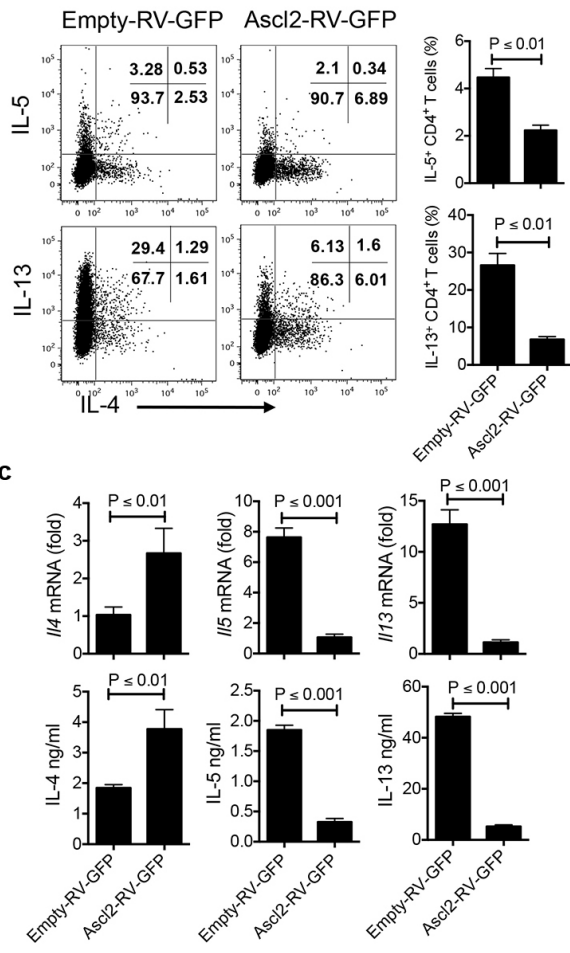
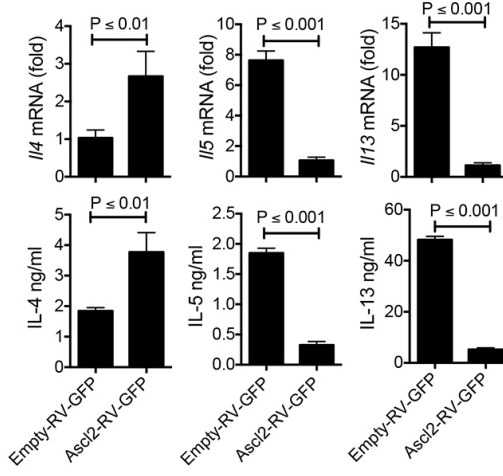
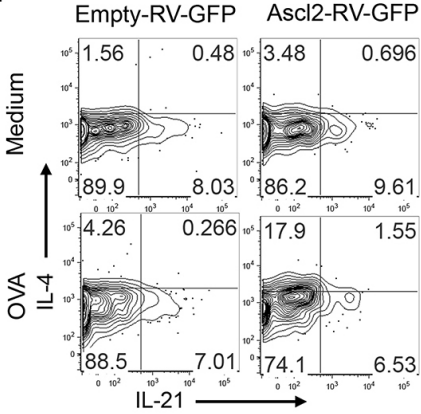
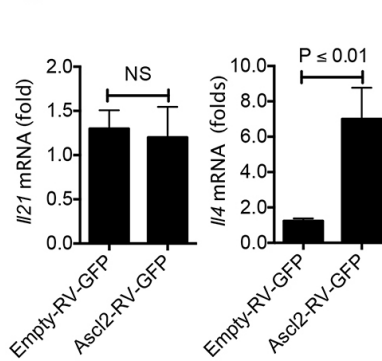
Extended Data Figure 1 | Ascl2 exhibits unique epigenetic regulation in T_{FH} cells, and its expression is dependent on Wnt signalling. **a**, Genome-wide histone modifications (H3K4me3, permissive marker; H3K27me3, suppressive marker) across *Bcl6*, *Maf*, *Batf*, *Irf4* and *Ascl2* loci in T-cell subsets (*in vivo* T_{FH} and non-T_{FH} data sets were newly generated; the rest were derived from the Gene Expression Omnibus database (accession GSE14254)²⁸). **b**, Flow cytometric analysis of *Ascl2* expression in three populations of activated CD44⁺CD4⁺ T cells in dLNs from *Bcl6-RFP* mice: CXCR5^{hi}*Bcl6*^{hi} (red), CXCR5⁺*Bcl6*^{lo} (blue) and CXCR5⁻*Bcl6*⁻ (black) cells. **c**, Quantitative RT-PCR measurement of *Ascl2*, *Bcl6* and *Batf* expression in *Bcl6-RV-GFP*,

Batf-RV-GFP and control vector-infected CD4⁺ T cells; wild-type (WT) and *Stat5*^{-/-} naive CD4⁺ T cells were cultured under T_{H0} conditions, or together with IL-6, respectively. *Ascl2*, *Bcl6* and *Batf* transcriptional expression was measured by qRT-PCR. **d**, Quantitative RT-PCR measurement of *Ascl2* in CD4⁺ T cells cultured under indicated conditions. **e**, Quantitative RT-PCR measurement of *Cxcr5* and *Bcl6* in control or TWS119- (1 μM) treated T cells. All experiments were repeated at least three times with similar results. Bar graphs show the relative level of mRNA as mean ± s.d., n = 3 per group. *P < 0.05, **P < 0.01, two-tailed t-test. NS, not significant.



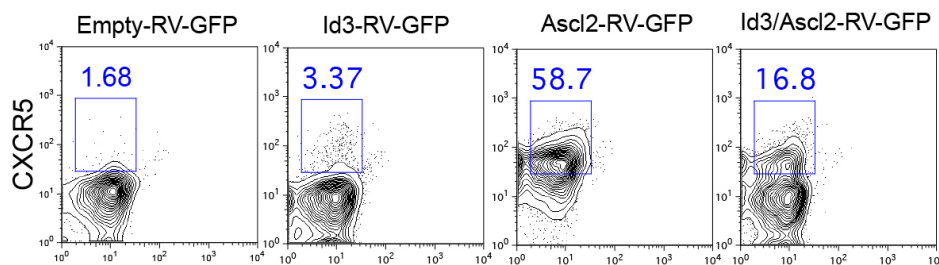
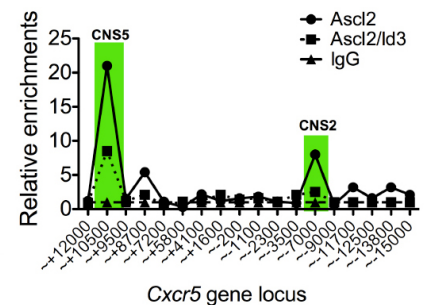
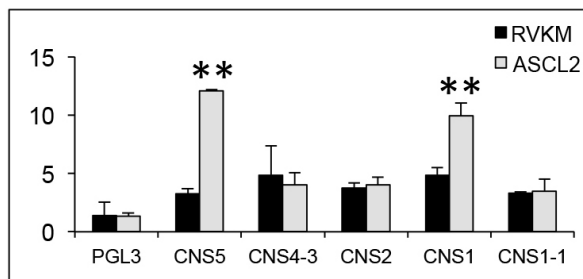
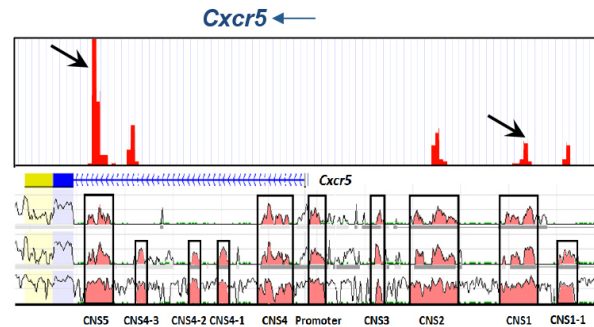
Extended Data Figure 2 | Ascl2 regulates a selective subset of T_{FH}-relevant genes. **a**, Flow cytometry analysis of CXCR5 expression in CD4⁺ T cells transduced with vector control, Ascl2-RV-GFP, Bcl6-RV-GFP, Batf-RV-GFP and Maf-RV-GFP. Data are representative of two independent experiments. **b**, Transcriptional expression of *Ccr7*, *Psgl1*, *Il2ra* and *Il2rb* in Ascl2-RV-GFP- or control-vector-infected T cells was measured by quantitative RT-PCR. Data are representative of two independent experiments. Bar graphs show the relative level of mRNA as mean ± s.d., $n = 3$, two-tailed *t*-test. **c**, Quantitative RT-PCR measurement of gene expression including the T_{H1}-related genes *Tbx21* and *Ifng*, as well as the T_{H17}-related genes *Rorc* and *Il17a*. Data are representative of three independent experiments. Bar graphs display the relative level of mRNA as mean ± s.d., $n = 3$, two-tailed *t*-test. **d**, Bcl6-RV-GFP- or control-viral-vector-infected GFP⁺ OT-II cells were adoptively

transferred into naive congenic mice, followed by subcutaneous OVA/CFA immunization. At day 2 after immunization, flow cytometry analysis of donor-derived cells in dLNs was carried out with CXCR5 and PD1 staining. Data are representative of two independent experiments ($n = 3$). **e**, Quantification of donor-derived T_{FH} cells. Bar graphs show mean ± s.d., $n = 3$, two-tailed *t*-test. NS, not significant. **f**, Vector-transduced GFP⁺CXCR5[−]CD4⁺ T (RV) cells, Ascl2-RV-GFP-infected GFP⁺CXCR5[−] (CXCR5[−]) and GFP⁺CXCR5⁺ (CXCR5⁺) CD4⁺ T cells were sorted and subjected to microarray assay. **g**, Hierarchical clustering and principal component analysis (PCA) were applied on seven microarray data sets including RV, CXCR5[−] and CXCR5⁺, as well as T_{FH} and non-T_{FH} cells (derived from GSE40068)⁴. **h**, The clustered heatmap of ~350 genes from RV, CXCR5[−], CXCR5⁺, T_{FH} and non-T_{FH} cells. The colour coding applies to gene expression level (\log_2) with 0 as a median.

a**b****c****d****e**

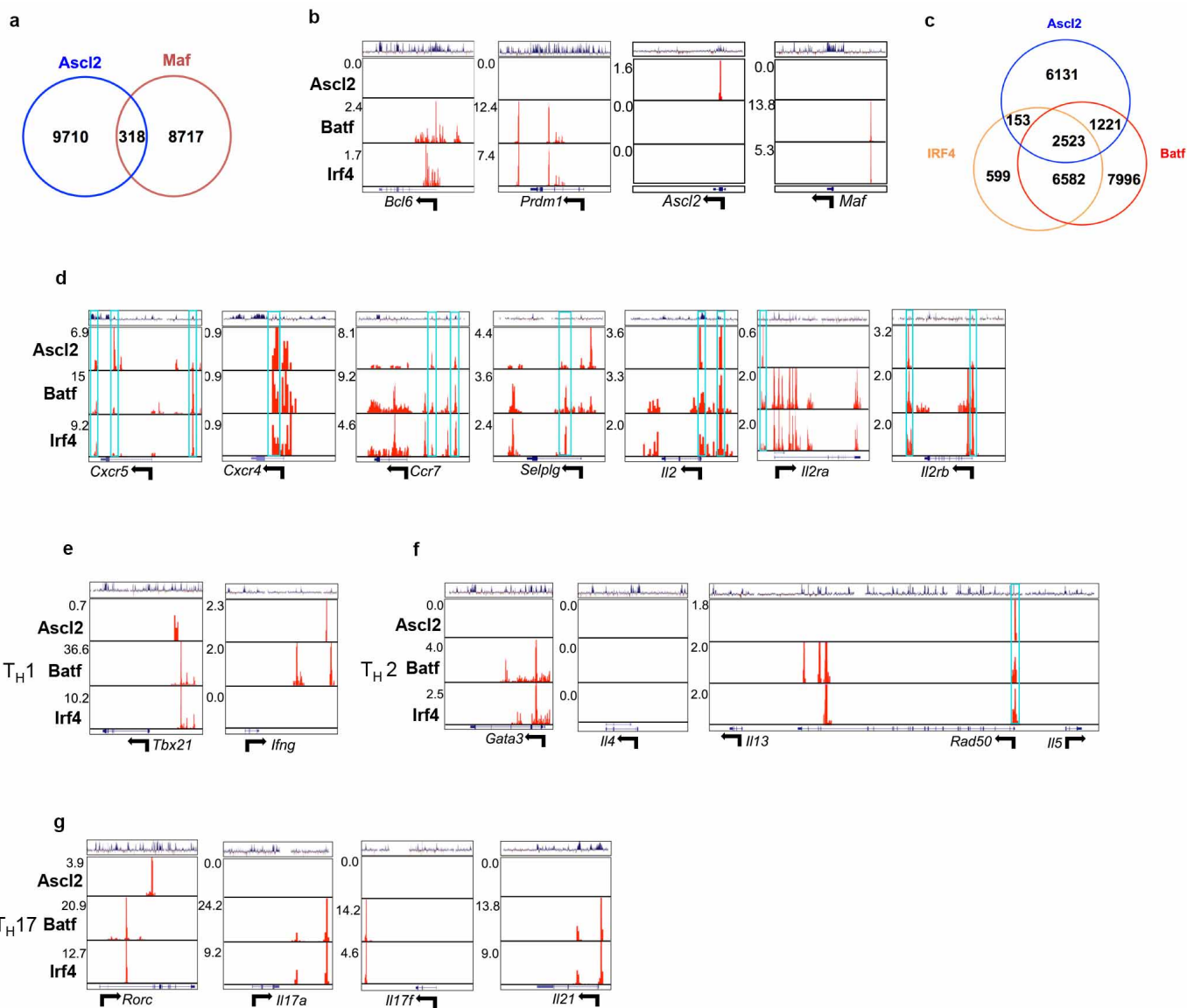
Extended Data Figure 3 | Regulation of T_H-cell differentiation by Ascl2. **a**, Naive CD4 $^{+}$ T cells from C57BL6 mice were activated under neutral conditions and infected with Ascl2-RV-GFP or control vector (empty-RV-GFP) virus, followed by continuous culture under T_H1, T_H2, T_H17, inducible (i)T_{reg} and T_{FH}-like conditions for 3–4 days. Quantification of signature genes by intracellular staining and real-time RT-PCR. **b**, **c**, Ascl2-RV-GFP- or control-vector-transduced T cells were cultured under T_H2 conditions for 4 days. **b**, After re-stimulation with PMA and ionomycin for 5 h, T_H2-related gene expression, including IL-4, IL-5 and IL-13, was measured by flow cytometric analysis. **c**, GFP $^{+}$ T cells were sorted and re-stimulated by plate-bound anti-CD3, and transcriptional expression of IL-4, IL-5 and IL-13 was

measured by quantitative RT-PCR; cytokines in supernatants from re-stimulation were subjected to ELISA analysis. **d**, **e**, Ascl2-RV-GFP- or control-vector-transduced OT-II cells were adoptively transferred into naive congenic mice, followed by subcutaneous OVA/CFA immunization for 7 days. **d**, After re-stimulation with OVA, flow cytometry analysis of donor-derived cells from dLNs was carried out with intracellular IL-4 and IL-21 staining. **e**, GFP $^{+}$ donor-derived T cells were sorted from dLNs, re-stimulated with anti-CD3, and subjected to quantitative RT-PCR measurement of *Il21* and *Il4* mRNA expression. All data are representative of two independent experiments. **a–c, e**, Bar graphs show mean \pm s.d., n = 3, two-tailed *t*-test. NS, not significant.

a**b****c****d**

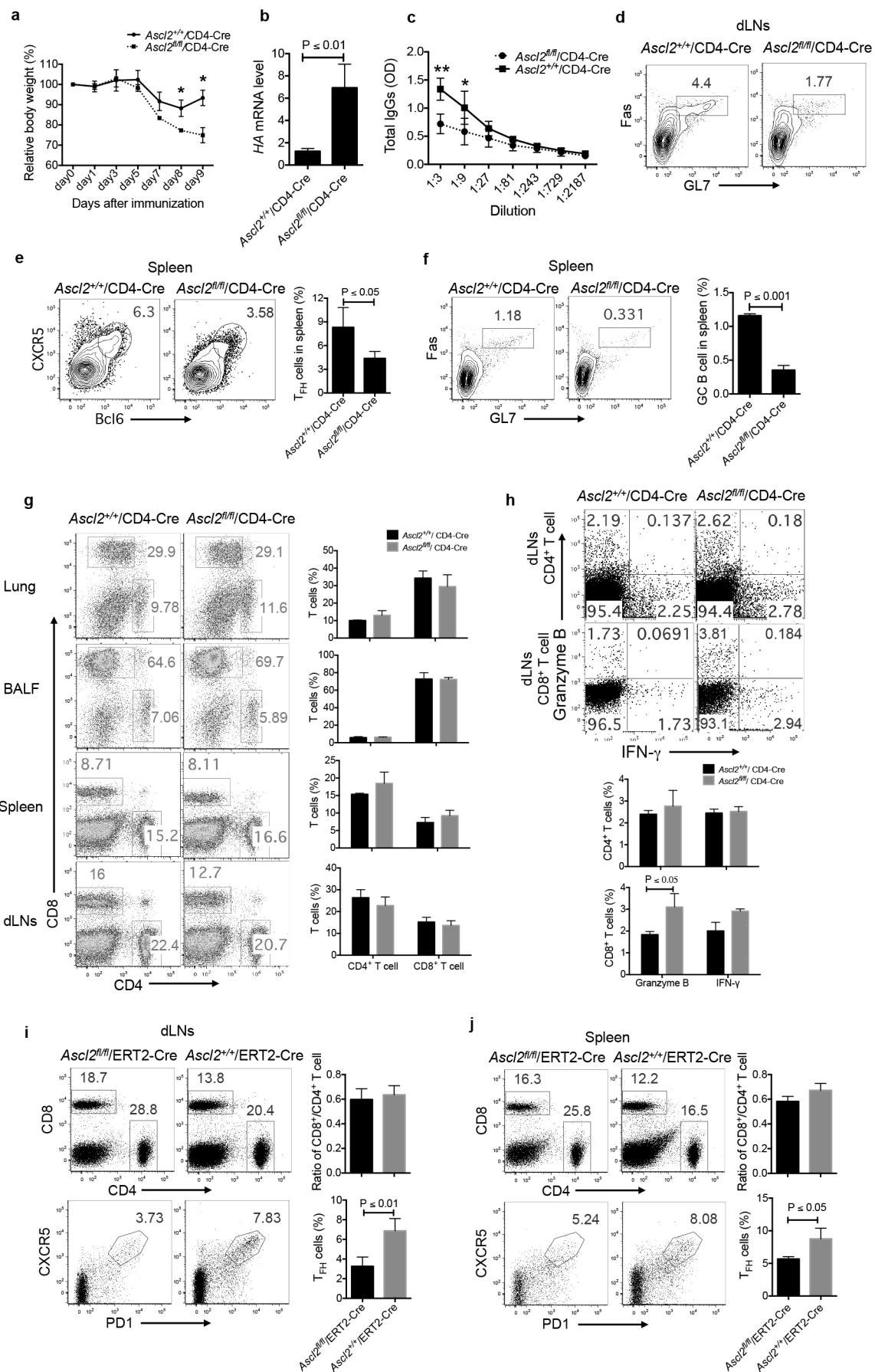
Extended Data Figure 4 | CXCR5 expression is directly mediated by Ascl2.
a, b, Naive CD4⁺ T cells were pre-activated and transduced with empty-RV-GFP, Id3-RV-GFP, Ascl2-RV-GFP or Ascl2-RV-GFP, together with Id3-RV-GFP retrovirus. **a**, Flow cytometry analysis of CXCR5 expression in retrovirus-infected T cells. Data are representative of two independent experiments. **b**, GFP⁺ cells were sorted from Ascl2-RV-GFP or Ascl2-RV-GFP plus Id3-RV-GFP retrovirus-infected T cells, and subjected to Ascl2-binding analysis of the *Cxcr5* gene locus using a ChIP assay. Primer information is listed

in Supplementary Table 2. Data are representative of two independent experiments. **c**, Luciferase reporter assay of enhancer activity for the Ascl2-bound region of the *Cxcr5* locus. CNS-containing PGL3 plasmid was transfected with either empty-RV-GFP or Ascl2-RV-GFP into the EL4 T-cell line. Bar graph shows mean \pm s.d., $n = 3$. ** $P < 0.01$, two-tailed *t*-test. **d**, Map of *Cxcr5* gene locus and Ascl2-binding peaks at the *Cxcr5* locus. Arrows indicate the Ascl2-responsive CNS region.



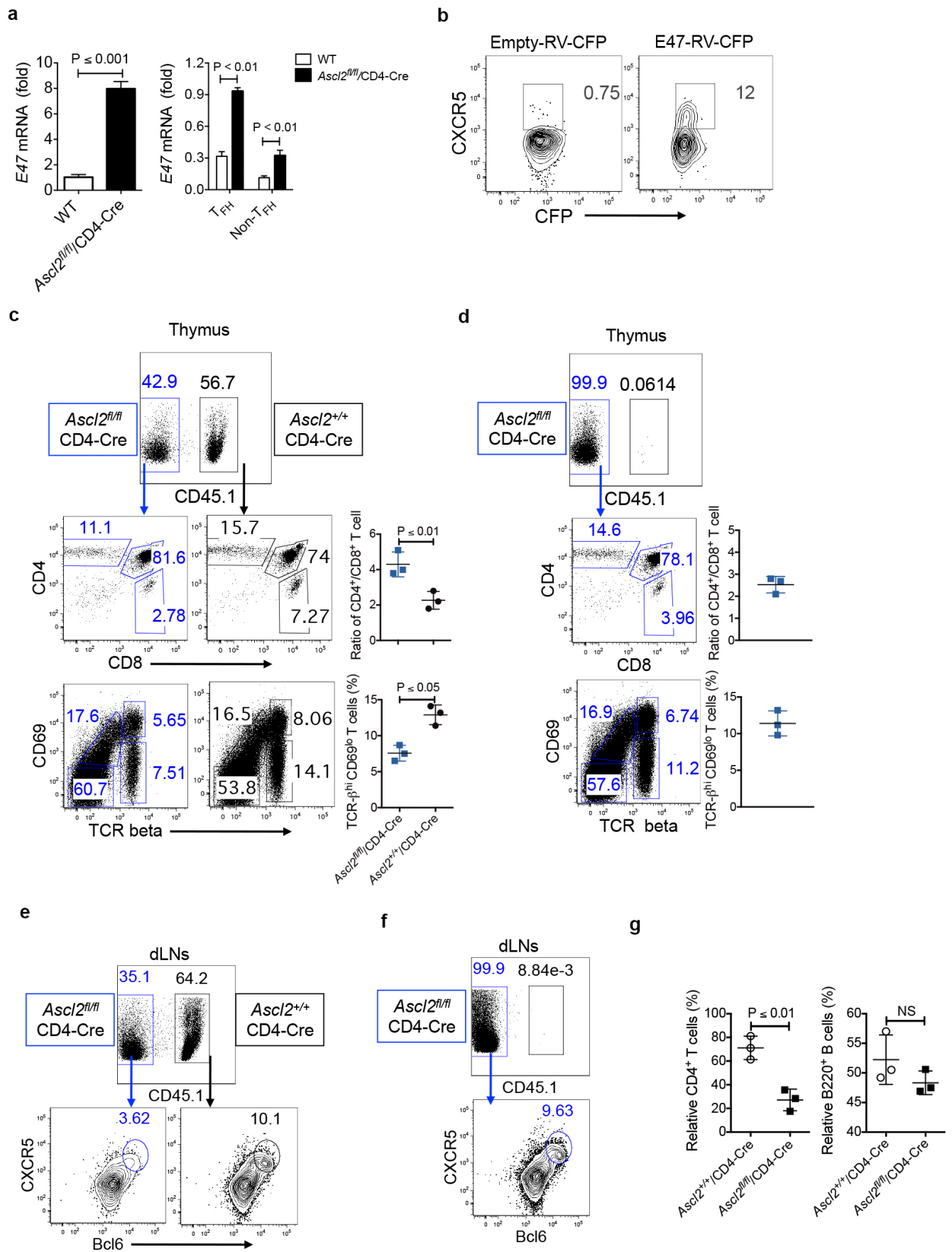
Extended Data Figure 5 | Coordinated function of Ascl2 and Batf/IRF4 in regulating T_{FH}-related genes. **a-g**, ChIP-Seq data for Maf, Batf and IRF4 were derived from GSE40918 (ref. 25). **a**, Venn diagram of ChIP-seq peaks from Ascl2 and Maf. **b**, Distribution of ChIP-seq peaks by Ascl2, Batf and IRF4 on gene loci including *Bcl6*, *Prdm1*, *Ascl2* and *Maf*. **c**, Venn diagram of ChIP-seq peaks from Ascl2, Batf and IRF4. **d**, Distribution of ChIP-seq peaks by Ascl2, Batf and IRF4 on gene loci including *Cxcr5*, *Cxcr4*, *Ccr7*, *Selplg1*, *Il2*, *Il2ra* and *Il2rb*. Blue frame represents the colocalization of peaks.

e, Distribution of ChIP-seq peaks by Ascl2, Batf and IRF4 on T_H1-related *Tbx21* and *Ifng* gene loci. **f**, Distribution of ChIP-seq peaks by Ascl2, Batf and IRF4 on T_H2-related *Gata3*, *Il4*, *Il13* and *Il5* gene loci. **g**, Distribution of ChIP-seq peaks by Ascl2, Batf and IRF4 on T_H17-related *Rorc*, *Il17a*, *Il17f* and *Il21* gene loci. ChIP-seq assay of Ascl2 was performed on Ascl2-overexpressing T cells cultured under T_H0 conditions. ChIP-seq assays of Maf, Batf and IRF4 were performed on T_H0 cells by D. R. Littman's group, derived from GSE40918 (ref. 25).



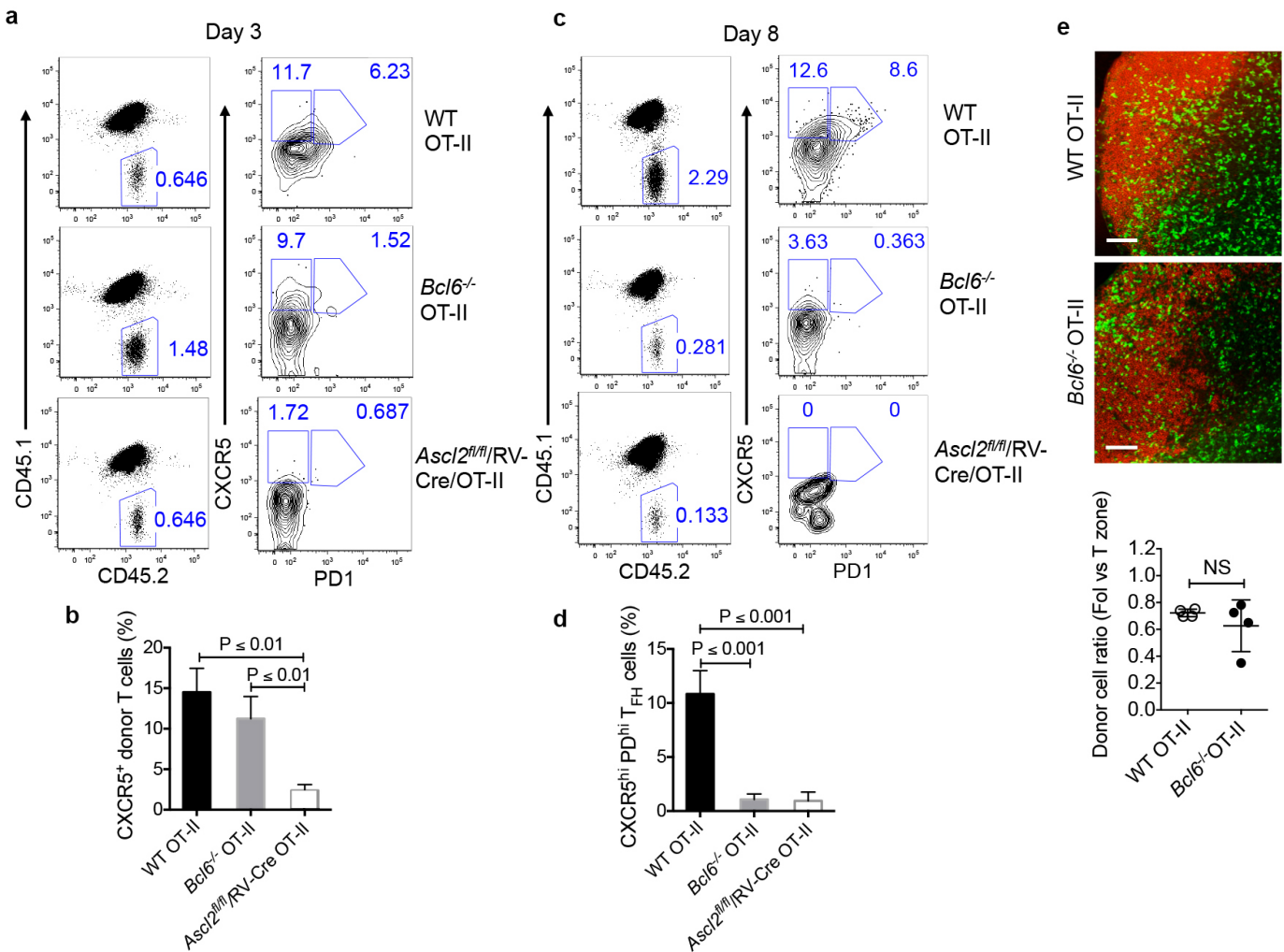
Extended Data Figure 6 | Loss of Ascl2 in CD4⁺ T cells leads to impairment of germinal centre responses during influenza virus infection. **a–j,** Control and *Ascl2^{fl/fl}/CD4-Cre* mice were infected intranasally with influenza virus A/PR8. **a,** The body weight of control and *Ascl2^{fl/fl}/CD4-Cre* mice was monitored daily after infection. **b,** Mice were killed at day 9 after infection, and viral titre in the lungs was assessed by measurement of active HA gene expression with quantitative RT-PCR. **c,** Virus-specific total IgGs in the sera were measured by ELISA. **d,** Flow cytometry analysis of germinal centre B cells (GL7^{hi}FAS^{hi}) in lung dLNs from influenza-infected control and *Ascl2^{fl/fl}/CD4-Cre* mice. **e,** Frequencies of T_{FH} cells in spleens from influenza-infected control and *Ascl2^{fl/fl}/CD4-Cre* mice. **f,** Frequencies of germinal centre B cells in spleens from influenza-infected control and *Ascl2^{fl/fl}/CD4-Cre* mice.

g, After 9 d.p.i., the CD4⁺/CD8⁺ T-cell ratio was measured in the lung, BALF, spleen and dLNs from control and *Ascl2^{fl/fl}/CD4-Cre* mice. **h,** Flow cytometry analysis of granzyme B and IFN- γ production from both CD4⁺ and CD8⁺ T cells in dLNs. **i, j,** Mixed chimaeric mice were reconstituted with both *Ascl2^{+/+}/ETR2-Cre* and *Ascl2^{fl/fl}/ETR2-Cre* bone marrow cells at a ratio of 1:1. Eight weeks later, chimaeric mice were administered 200 μ l tamoxifen (5 mg ml⁻¹) in sunflower seed oil i.p. every other day for a total of 5 days, and this was followed by influenza virus A/PR8 infection. At 9 d.p.i., the CD4⁺/CD8⁺ T-cell ratio and T_{FH}-cell generation was measured in dLNs (**i**) and spleens (**j**). All data are representative of three independent experiments. Graphs display mean \pm s.d., $n = 5$ per group. * $P < 0.05$, ** $P < 0.01$, two-way ANOVA (**a, c**), two-tailed *t*-test (**b, e, f, g–j**). NS, not significant.



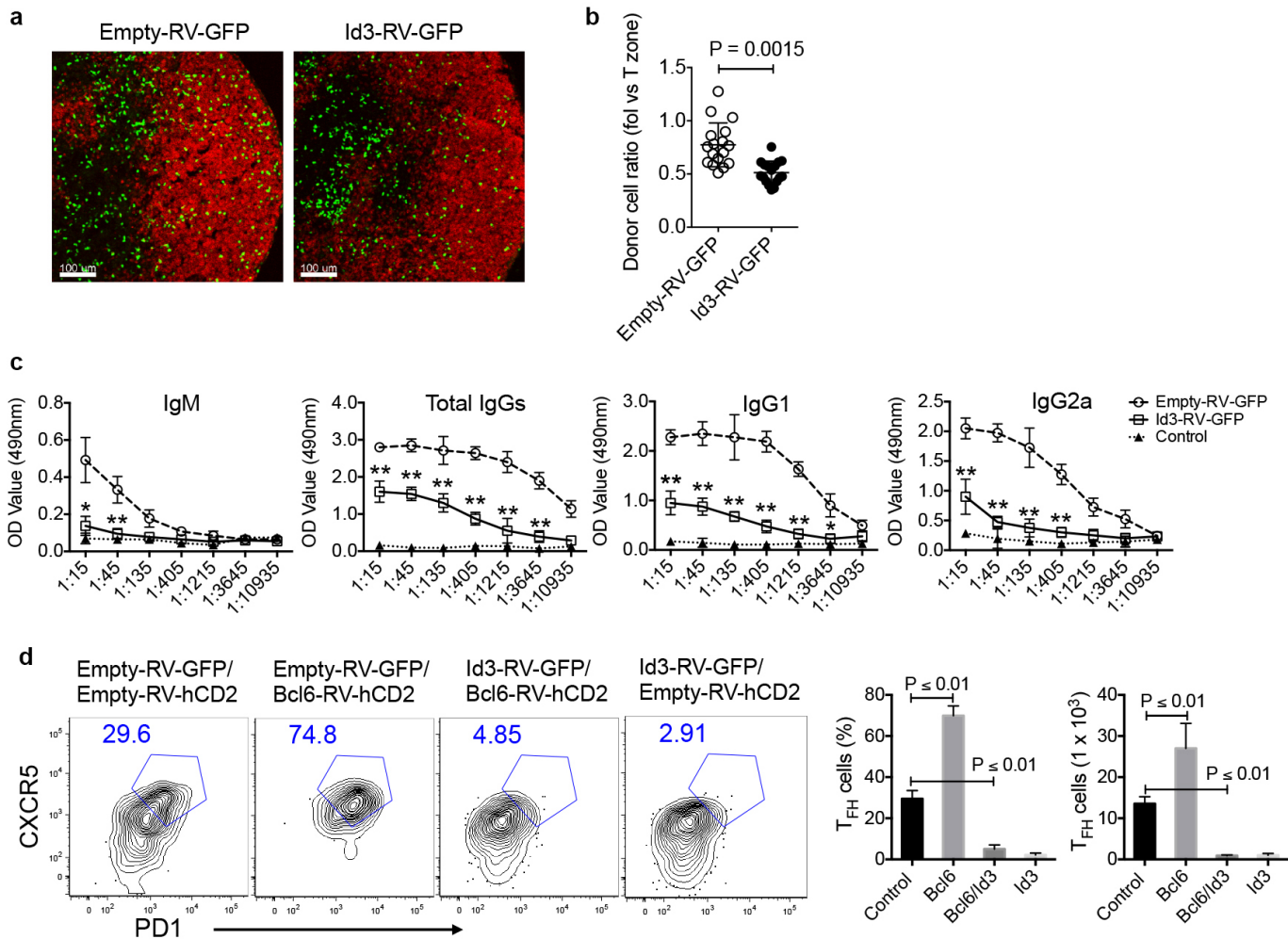
Extended Data Figure 7 | In the absence of Ascl2, bHLH family member E47 may have a redundant role in T_{FH}-cell differentiation. **a**, Quantitative RT-PCR measurement of E47 expression in naive CD4⁺ T cells from *Ascl2^{fl/fl}/CD4-Cre* and littermate control mice; T_{FH} and non-T_{FH} cells were obtained from dLNs of *Ascl2^{fl/fl}/CD4-Cre* and littermate control mice immunized with KLH in CFA, and the expression of *E47* was measured by real-time RT-PCR. **b**, Flow cytometry analysis of CXCR5 expression in T cells infected with E47-RV-CFP or control vector retrovirus. **c–g**, T-cell-depleted bone marrow cells were obtained from *Ascl2^{+/+}/CD4-Cre* (CD45.1⁺ CD45.2⁺) and *Ascl2^{fl/fl}/CD4-Cre* (CD45.2⁺) mice and mixed at a ratio of 1:1 or 0:1 before being transferred into irradiated *Rag1^{-/-}* recipient mice (8×10^6 cells per mouse). **c–g**, Eight weeks later, mice were either used for measurement of thymic T-cell maturation (**c, d**), or immunized with KLH in CFA for monitoring peripheral

T_{FH}-cell differentiation (**e–g**). **c**, Flow cytometry analysis of T-cell maturation in thymus of mixed chimaeric mice containing both *Ascl2^{+/+}/CD4-Cre* and *Ascl2^{fl/fl}/CD4-Cre* bone marrow cells. **d**, Flow cytometry analysis of T-cell maturation in thymus of chimaeric mice containing only *Ascl2^{fl/fl}/CD4-Cre* bone marrow cells. **e**, Seven days after immunization, T_{FH} cells in dLNs of mixed chimaeric mice (*Ascl2^{+/+}/CD4-Cre* and *Ascl2^{fl/fl}/CD4-Cre*) were measured by flow cytometry. **f**, Flow cytometry analysis of T_{FH} cells in dLNs of chimaeric mice (*Ascl2^{fl/fl}/CD4-Cre*). **g**, The percentages of both CD4⁺ T cells and B220⁺ B cells in dLNs of mixed chimaeric mice (*Ascl2^{+/+}/CD4-Cre* and *Ascl2^{fl/fl}/CD4-Cre*). All data above are representative of two independent experiments. Graphs show mean \pm s.d., $n = 3$ per group, two-tailed *t*-test. NS, not significant.



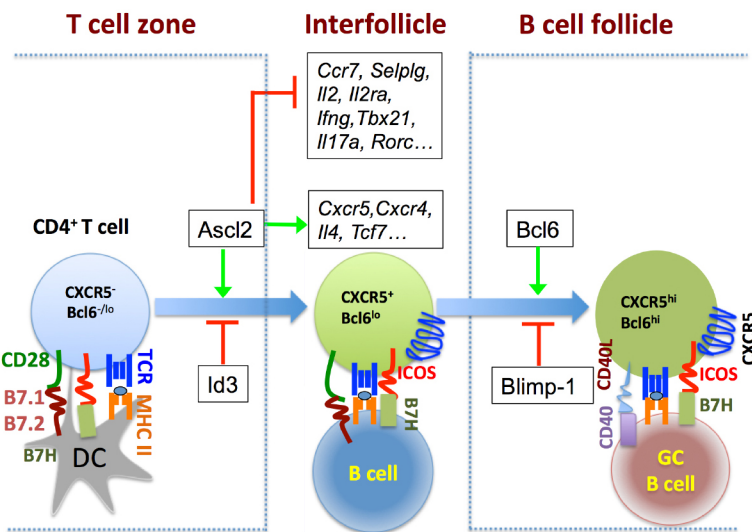
Extended Data Figure 8 | Loss of Bcl6 in CD4⁺ T cells does not affect early T_{FH}-cell homing ability *in vivo*. Equal amounts of Cre-RV-GFP-transduced wild-type (WT)/OT-II, Bcl6^{-/-}/OT-II and Ascl2^{fl/fl}/OT-II cells were transferred into congenic mice, and this was followed by subcutaneous OVA/CFA immunization. **a**, At day 3 after immunization, flow cytometry analysis of donor-derived T_{FH}-cell generation was carried out with CXCR5 and PD1 staining. **b**, Quantification of donor-derived CXCR5⁺ T cells. **c**, At day 8 after

immunization, donor-derived T_{FH}-cell generation was examined using CXCR5 and PD1 staining. **d**, Quantification of donor-derived CXCR5⁺ PD1⁺ T_{FH} cells. **e**, At day 3 after immunization, dLNs were isolated and subjected to histochemical staining of B-cell follicles and donor T cells. Green, GFP; red, B220; scale bar, 100 μm, $n = 4$. All data are representative of two independent experiments. Graphs display mean ± s.d., $n = 4$, two-tailed *t*-test, NS, not significant.



Extended Data Figure 9 | Ectopic expression of Id3 inhibits T_{FH}-cell generation *in vivo*. **a–c.** Naive OT-II CD4⁺ T cells were activated and transduced with Id3-RV-GFP or control viral vector (empty-RV-GFP) for 3 days. GFP⁺ T cells were then sorted and transferred into naive congenic mice that were subsequently immunized with OVA/CFA. **a.** At day 4 after immunization with OVA/Alum/LPS, immunohistochemical staining of section slides of dLNs was carried out. Red, IgD⁺ B cells; green, GFP⁺ donor-derived OT-II cells. Data are representative of two independent experiments, $n = 6$. Scale bar, 100 μ m. **b.** Quantification of GFP⁺ OT-II cell distributions in dLNs. Data are representative of two independent experiments. Dot graph shows mean \pm s.d., $n = 17$, two-tailed *t*-test. **c.** Optical density (OD) values of

OVA-specific antibodies in serum from mice on day 7 after immunization with OVA/CFA, measured by threefold serial dilution in OVA- (100 μ g ml⁻¹) coated plates. Data are representative of two independent experiments. Graphs show mean \pm s.d., $n = 6$. **P* < 0.05, ***P* < 0.01, one-way ANOVA. **d.** Naive CD4⁺ OT-II cells were pre-activated and co-transduced with empty-RV-GFP/empty-RV-hCD2, empty-RV-GFP/Bcl6-RV-hCD2, Id3-RV-GFP/Bcl6-RV-hCD2, or Id3-RV-GFP/empty-RV-hCD2. Sorted hCD2⁺GFP⁺ OT-II cells were transferred into congenic mice, followed by subcutaneous OVA/CFA immunization for 7 days. Measurement of donor-derived T_{FH} cells was carried out with CXCR5 and PD1 staining. Data are representative of two independent experiments. Bar graphs show mean \pm s.d., $n = 3$, two-tailed *t*-test.



Extended Data Figure 10 | Schematic model of the sequential roles of Ascl2, Id3 and Bcl6/Blimp1 during T_{FH}-cell differentiation. Ascl2 expression plus simultaneous Id3 reduction in activated CD4⁺ T cells orchestrates T cells to migrate towards B-cell follicles and initiate the T_{FH} program by inducing expression of the chemokine receptors CXCR5 and CXCR4, and suppressing

expression of CCR7 and PSGL1 and the IL-2 signal pathway, as well as T_H1 and T_H17 differentiation. Upon interacting with cognate B cells at the T-B border, CXCR5⁺ T cells begin to increase Bcl6 expression, which eventually facilitates T_{FH} maturation in B follicles and germinal centre formation.